Preliminary hydrogeological characterisation of the Sakete plateau in the coastal sedimentary basin of Benin

Auteur : Durieux, Simon
Promoteur(s) : Brouyere, Serge
Faculté : Faculté des Sciences appliquées
Diplôme : Master en ingénieur civil des mines et géologue, à finalité spécialisée en géologie de l'ingénieur et de l'environnement
Année académique : 2021-2022
URI/URL : http://hdl.handle.net/2268.2/16543

University of Liège - School of Engineering and Computer Science

Preliminary hydrogeological characterisation of the Sakété plateau in the coastal sedimentary basin of Benin

Master's thesis carried out to obtain the degree of Master of Science in Geological and Mining Engineering

Simon Durieux

Supervisor : Dr. Serge Brouyère

Academic year 2021-2022

Acknowledgement

This thesis was a great learning experience that gave me the opportunity to travel to Benin and directly collect the data needed to conduct it. I have to thank my supervisor Dr. Serge Brouyère for this opportunity and for his expertise and advices during the analysis of the data and the redaction of the thesis. I would also like to thank Philippe Orban and Frédéric Nguyen for their help.
I also thank the people who welcomed and accompanied me during my stay in Benin, Thierry Helsens, Christian Allé and Fabrice Lawson.

Finally, I would like to thank my friends and family, which supported me during the redaction of this thesis. A special thanks need to be addressed to the two friends that accompanied me during all of my studies, Nicolas Gianfolcaro and Nicolas Massaux, and to the one that convinced me to change my focus from computer science to geology, Guillaume Bottin.

Abstract

The aim of this thesis is to conduct a preliminary hydrogeological characterization of the Sakété plateau in the coastal sedimentary basin of Benin in terms of groundwater quantity, more precisely of the Mio-Pliocène aquifer of the plateau.

To do so, the results of geophysical surveys (Time-domain electromagnetic (TDEM) and Magnetic Resonance Sounding (MRS)) and water samples collected on site during an internship in Benin, the hydrogeology and hydrochemistry of the Sakété plateau were analysed and compared to the existing results on the Allada plateau.
Using data from the NASA POWER project, the precipitations were also analysed to estimate the effective water on both the Sakété and Allada plateaus.

The analysis of these data showed that although the geology and piezometric levels of both plateaus are similar, they differ in their ionic concentrations and in the amount of water that is absorbed by the soil. The Sakété plateau receives more water and more water can be absorbed by the soil, thus extrapolating the results from the Allada plateau to the Sakété plateau appear to be a conservative assumption as a primary hypothesis.

L'objectif de cette thèse est de réaliser une caractérisation hydrogéologique préliminaire du plateau de Sakété, dans le bassin sédimentaire côtier du Bénin, en termes de quantité d'eau souterraine, et plus précisément de l'aquifère Mio-Pliocène du plateau.

Pour ce faire, à partir des résultats de levés géophysiques (Time-domain electromagnetic (TDEM) et Magnetic Resonance Sounding (MRS)) et d'échantillons d'eau prélevés sur place lors d'un stage au Bénin, l'hydrogéologie et l'hydrochimie du plateau de Sakété ont été analysées et comparées aux résultats existants sur le plateau d'Allada.
En utilisant les données du projet POWER de la NASA, les précipitations ont également été analysées afin d'estimer l'eau utile sur les plateaux de Sakété et d'Allada.

L'analyse de ces données a montré que si la géologie et les niveaux piézométriques des deux plateaux sont similaires, ils diffèrent par leurs concentrations ioniques et par la quantité d'eau absorbée par le sol. Le plateau de Sakété reçoit plus d'eau et plus d'eau peut être absorbée par le sol, donc l'extrapolation des résultats du plateau d'Allada au plateau de Sakété semble être une hypothèse conservatrice comme hypothèse primaire.

Contents

List of Figures

1 Introduction

1.1 Exposition of the problem

In Benin, management of the water resources is a problem of utmost importance. Indeed, the majority of the drinking water comes from the subsurface, with 43.2% coming from wells and only 13.8% coming from the surface (Balk et al. 2003).
Furthermore, the numerous wells and boreholes used to pump water haven't always sufficient flows in relation to the demands. According to Achidi et al. 2012a, the success rate of boreholes, computed as the number of positive boreholes (i.e. boreholes with an exploitable flow rate greater than $0.7m^3/h$, the minimum flow rate required for a village borehole operated by a human powered pump) in the coastal sedimentary basin is the greatest, with 90% of the boreholes being positive (the other sedimentary basin of Kandi and Volta having 81 and 71%, respectively, while the crystalline bedrock only has 62% of positive boreholes).

Being near the coast, the aquifers of the coastal sedimentary basin are prone to intrusion of salt water. The Godomey field, which supplies the population of Cotonou since 1956 in fresh water, is a prime example. Due to the increased pumping to sustain the growing population, it has seen its water level decreasing and its salinity increasing. Thus, several boreholes were abandoned, and a second well field was created in Ouédo in 2014, further away from the sea (IGRAC 2021).

With the current growth of cities such as Cotonou, Porto-Novo or Abomey Calavi, the pressure on the coastal aquifers is also increasing and the question of their management is becoming more and more important.
It is thus needed to know the quantity of available water and the recharge of the aquifers of the south of the country to make decisions concerning the use of the water and the protection of this precious resource.

This thesis focuses on the Sakété plateau and tries to characterize its hydrogeology and compare it with the Allada plateau based on data that were obtained during an internship in Benin with the DGEau (*Direction Générale de l'Eau*) and the INE-UAC (*Institut National de l'Eau de l'Université d'Abomey Calavi*), in the context of the project "Appui à la gestion durable et à l'exploitation des ressources en eau du Bénin pour l'AEP et l'agriculture irriguée", financed by the Commission Mixte Permanente Wallonie-Bruxelles International - Benin 2019-2023, of which the Hydrogeology and Environmental Geology team of the University of Liège is a partner.
To further characterize the hydrogeology of the plateau, data from the NASA Langley Research Center POWER Project (funded through the NASA Earth Science Directorate Applied Science Program) were also used.

1.2 Context of the internship with the DGEau and INE

The Omi-Delta project was created as a renewal of the cooperation between the Netherlands and Benin in the water and sanitary sector, funded by the Netherlands to the tune of 21 892 598 250 CFA francs (33 483 996 euros) (Synoptic file of the Omi-Delta project, Ministère de l'Eau et des Mines du Bénin 2020). This project is leaded by the DGEau and is technically assisted by the INE-UAC.
One of its aim is to improve water management in the Ouémé Delta. To do so, a characterization of the groundwater resource is needed on the two plateaus adjacent to the Ouémé valley, the Allada plateau (to the west), and the Sakété plateau (to the east).

The Allada plateau is currently being characterized as part of the Omi-Delta project, and the Sakété plateau should be characterized in the future. However, the ongoing study has shown similar piezometric levels between both plateaus, which suggest that the Mio-Pliocène aquifer of both plateaus may be interconnected. If they are, a first hypothesis can be made to have an idea of the available groundwater resource in the Sakété plateau based on the results of the study of the Allada plateau.

The aim of the internship was to collect data to confirm this hypothesis. Three types of data were gathered : Magnetic Resonance Sounding (MRS), Time Domain Electromagnetic (TDEM) and water samples analysed later in Belgium.

2 General context

2.1 Geography

The study region is the Sakété plateau, which is situated in the southern part of Benin, up north of the capital, Porto-Novo, as shown on the Figure 1 in red. It spans over two departments : Plateau and Ouémé, and covers about $1500 km^2$.
The topography varies from 0 to 160m, with the higher elevation being in the north, near Pobè and the lowest in the south, near Porto-Novo. The Figure 2 shows the topography of the south of Benin, the Ouémé valley (west of the plateau) and the Lama depression (north of the plateau) are clearly visible.
The major cities in the region are Cotonou (the economic capital) and Porto-Novo (the official capital).

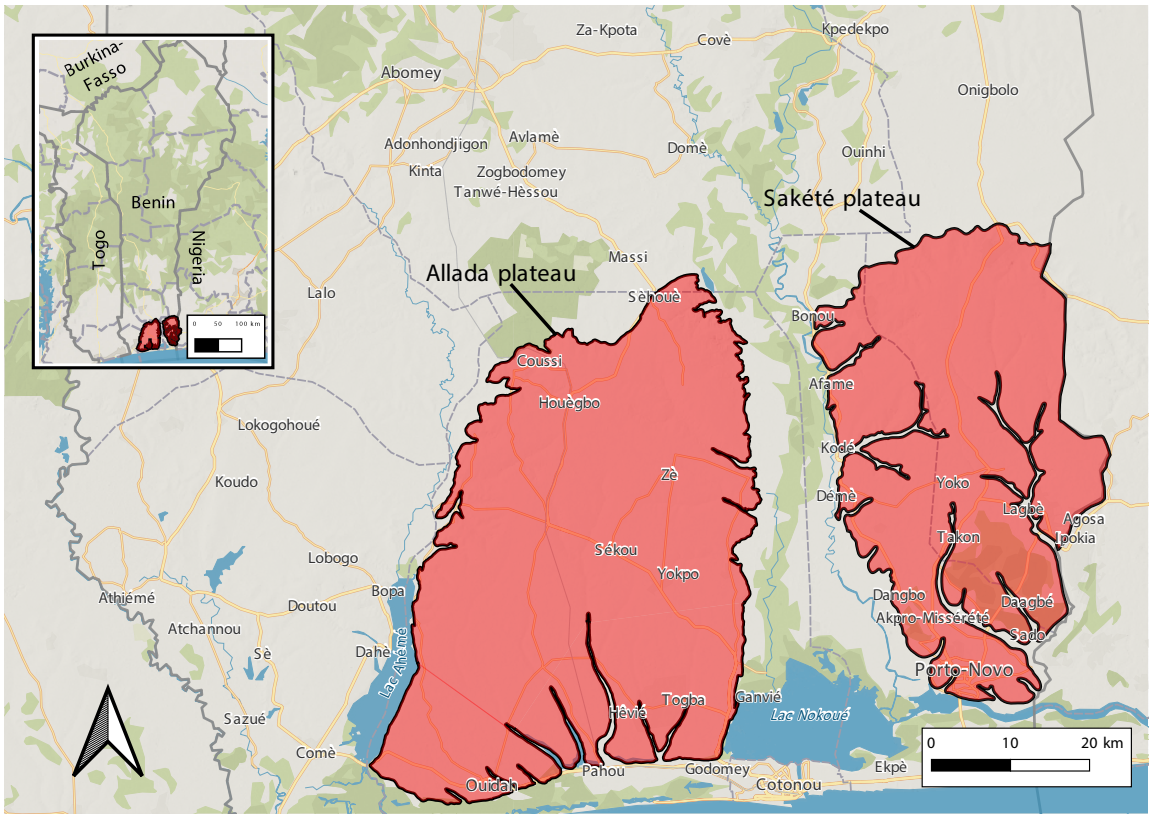

Figure 1: Map of Benin (in the up left corner) and a zoom on the coastal sedimentary basin, with the Sakété and Allada plateaus in red

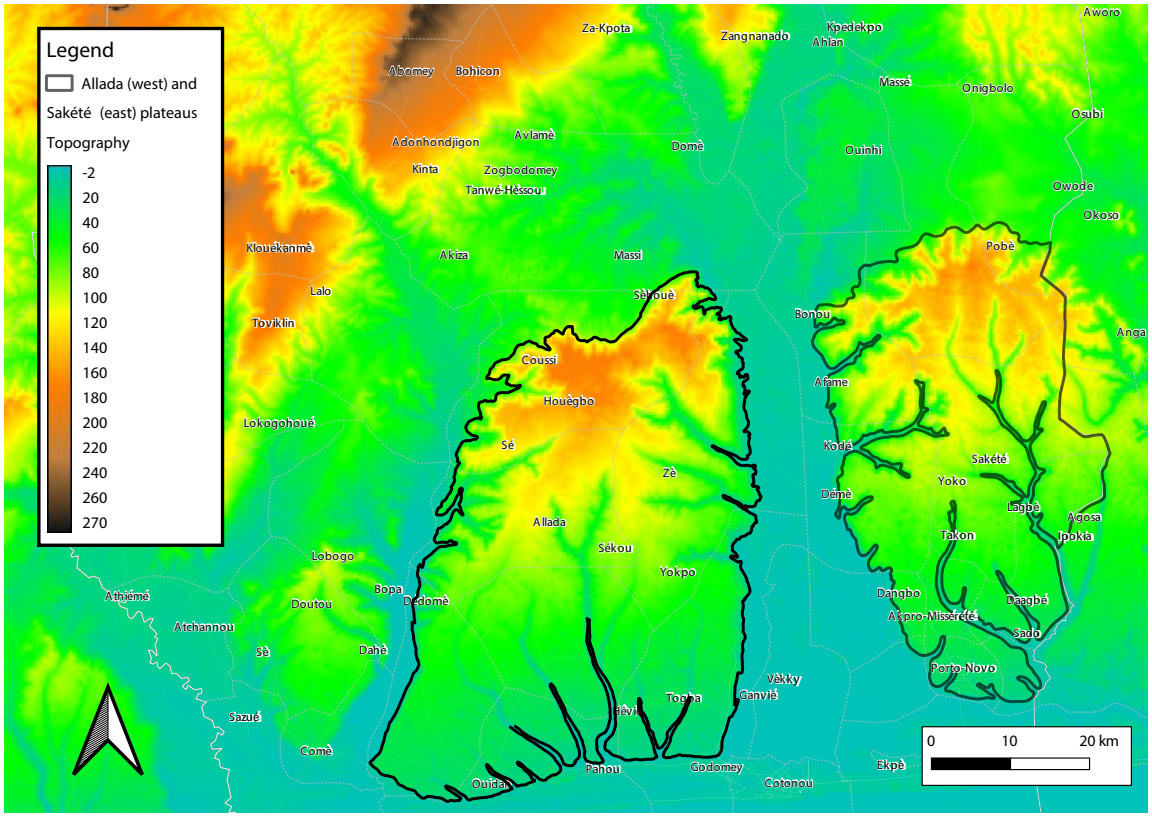

Figure 2: Topography of the south of the Benin, modified from Global Multi-Resolution Terrain Elevation Data, Danielson and Gesch 2011

2.2 Climate

The Sakété plateau is located in the sub-equatorial region, and has two rainy seasons : a first one from March to July and a shorter one from September to November. The mean annual rainfall for the Plateau and Ouémé departments between 1991 and 2020 are respectively 1149.08 and 1219.77 mm with a mean temperature of 27.71°C. For the same time period, the maximum temperatures can reach 32°C, while the lowest temperatures are about 23°C. (The World Bank Group 2021).
The mean relative humidity is relatively high, about 83%, and can vary between 60% and 90%.

The Figure 3 shows the isohyet map of the whole country for the period of 1950 to 2010. Looking at the southern part of the map, it appears that the Sakété plateau has more precipitation than the Allada plateau, a gradient of precipitation can be observed from west to east in this part of Benin, ranging from 900 to 1200 mm/year.

A further analysis of the climate of Benin will be made with the NASA POWER data in the section 3.3.

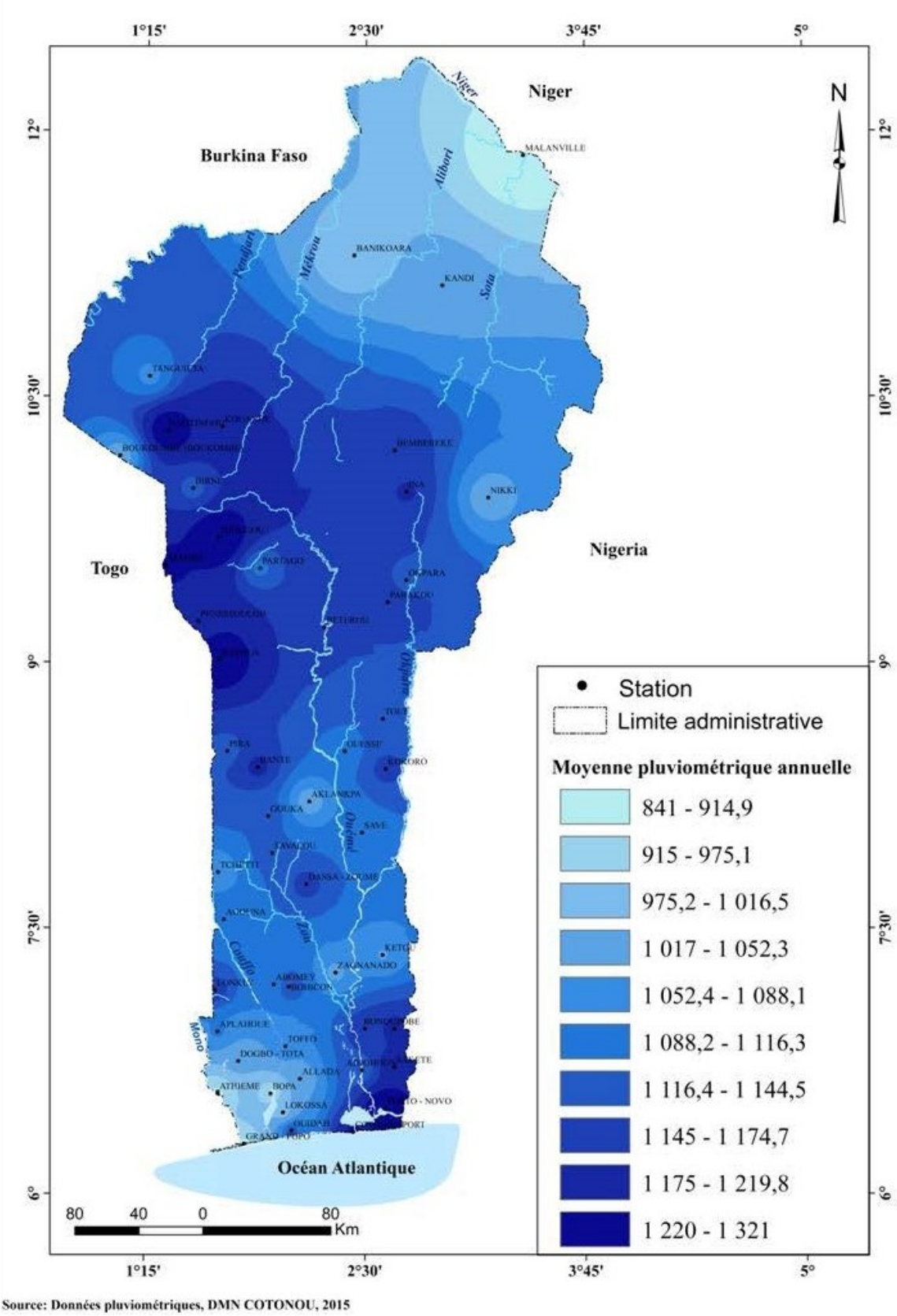

Figure 3: Isohyet map for the period 1950-2010 (Amoussou et al. 2016)

2.3 Geomorphology

The studied region is a plateau oriented WSW-ENE, delineated in the south by the Atlantique Ocean and a swampy area (where Cotonou is located), in the west by the Ouémé valley, in the east by the Nigerian border and up north by the Lama depression (Achidi et al. 2012b).
The following map (Figure 4) shows the different plateaus, depression and valleys of the south of Benin. These features can also be seen on the topographical map on the Figure 2.

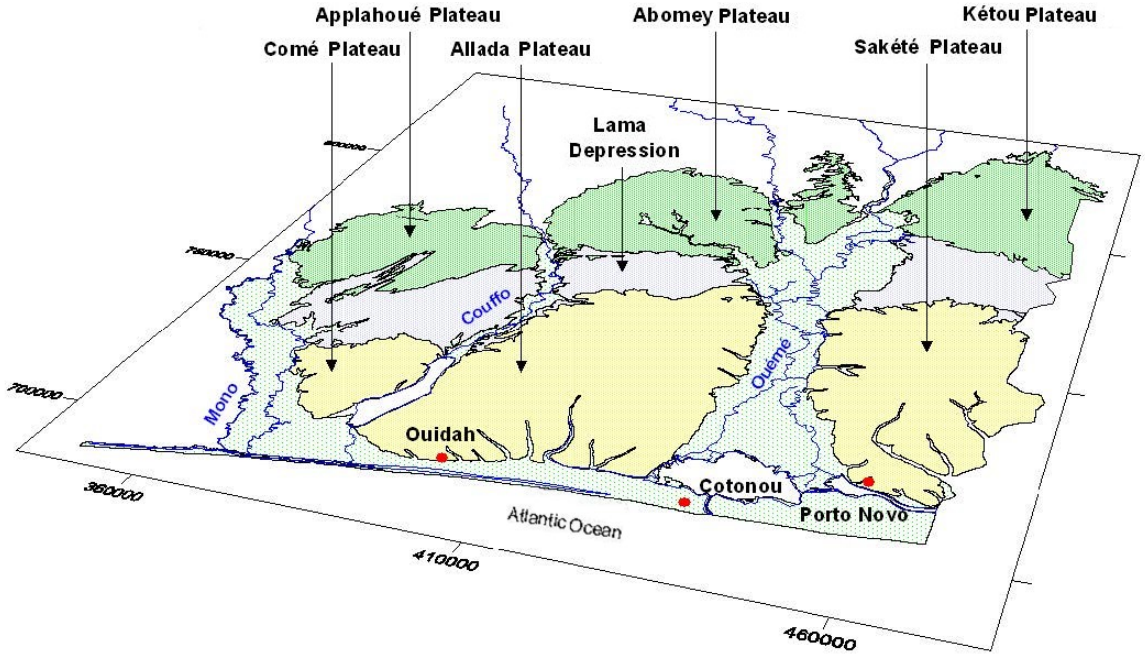

Figure 4: Geomorphological map of the coastal sedimentary basin of Benin (translated from Achidi et al. 2012b)

2.4 Land use / Vegetation

The vegetation in the studied area was impacted a lot by the anthropic activities. The result is a large portion being plantations (palm trees, coco tree, manioc...) and savana with small patches of classified and sacred forest that are protected and close to the original semi-deciduous tropical forests (Alohou et al. 2017, Sokpon 1995).

2.5 Soils

The main soils in the studied area are Acrisols, Vertisols and Ferric luvisols (Kindohoundé et al. 2021), which are defined by the Food and Agriculture Organization of the United Nations 2006 as strongly weathered soils with a high clay content.

2.6 Hydrology

The surface hydrology in the south of Benin can be summarized as rivers flowing into alluvial plains that separates the different plateaus, with some of their tributaries running across the plateaus and in the south of the plateaus a swampy area bordered by the coast where lakes (Lake Nokoué and Ahémé) and lagoons (Porto-Novo lagoon) can be found.

The main river of the studied region is the Ouémé, bordering the west side of the Sakété plateau. The smaller Gli-Awoyo borders the east side of the plateau.
Some tributaries of those rivers cross the plateau :

- The tributaries of the Ouémé : the Zou, the Gbadohouin, the Tovè and its own tributary, the Saoro;
- The tributaries of the Gli-Awoyo : the Koulé, the Anadomè, the Iguidi and the Assissa.

The map in Figure 5 shows the geographic distribution of the different rivers crossing the plateau.

The Ouémé is a 523 km long river, of which only the end, the delta of the Ouémé, is included in the studied region. The upper part of the delta has almost no water coming from the underground. Afterward, around Affame (at the beginning of the river Sô in Figure 5), the Ouémé becomes draining (which can be observed by the difference in flow during the low water months between the Bonou and Hétin-Sota stations, respectively 11.2 and 29.2 m^3/s). There, the Ouémé has multiple interactions with the Sô river, with a floodplain of 3.5 km on the left bank of the river (Le Barbé et al. 1993).
At the station of Bonou (upper left of the Sakété plateau), for the period 1987-2016, the highest flow rate are observed during August, September and October (which corresponds to the rainy season), with a pike in September of 753 m^3/s. This period corresponds to 80% of the annual flow rate, as the other months have an average flow rate around 10 m^3/s (and 200 m^3/s in July and November) (Cocker, Vodounou, and Yabi 2019).

The Nokoué lake is connected to the sea by the channel of Cotonou, which influences its salinity. During the rainy season, the high water levels stop the saline water intrusion, but during the dry season the inflow of seawater into the lake becomes significant and even exceeds the outflow of lagoon water, and the lakes becomes richer in salt, with a top to bottom gradient of the salt concentration (Le Barbé et al. 1993).

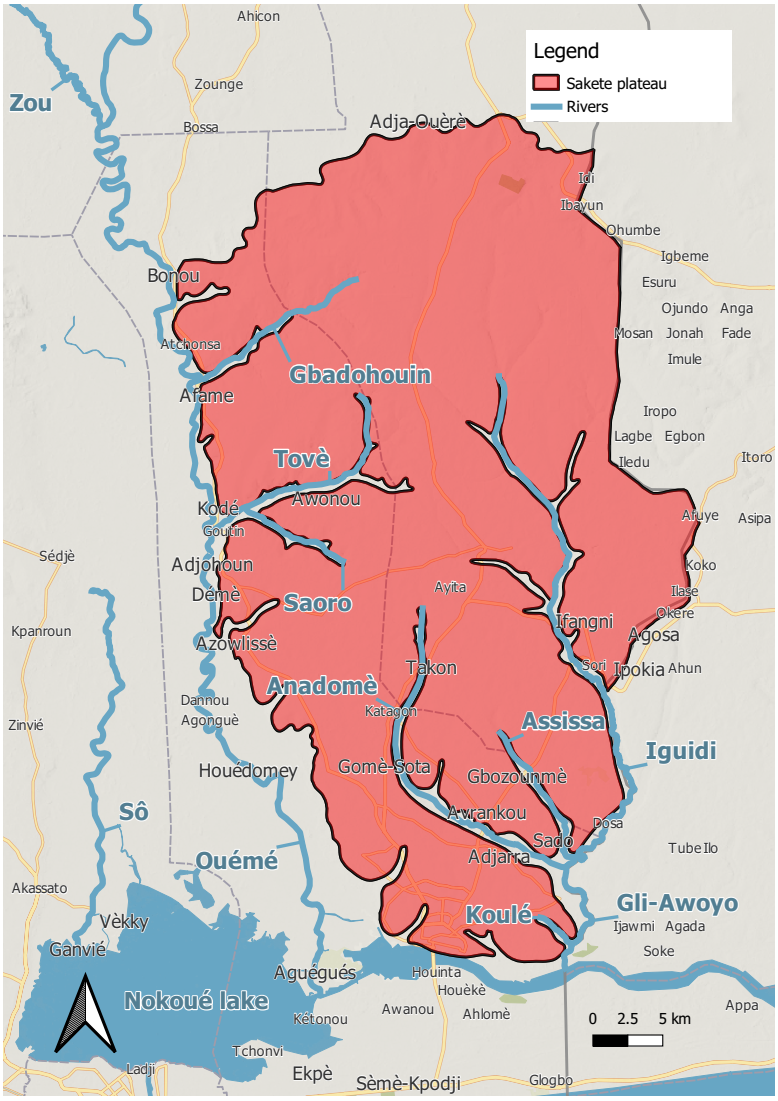

Figure 5: Map of the Sakété plateau (in red) with the main rivers and their names

2.7 Geology

The coastal sedimentary basin of Benin is a sedimentary deposit located on top of a crystalline bedrock. As shown in the Figure 6, on the Sakété plateau, the exposed formations are mainly from the Miocene, with some Eocene appearing in the north.
The geological cross-section in Figure 7 shows the different geological units and their corresponding number. The globally horizontal structure with a slight inclination towards the south is visible, with some faults in the north of the Allada plateau. The lithology of the formations is also visible, with the plateau being mainly sand and gravels on top of a silty and clayey substratum with a limestone layer.

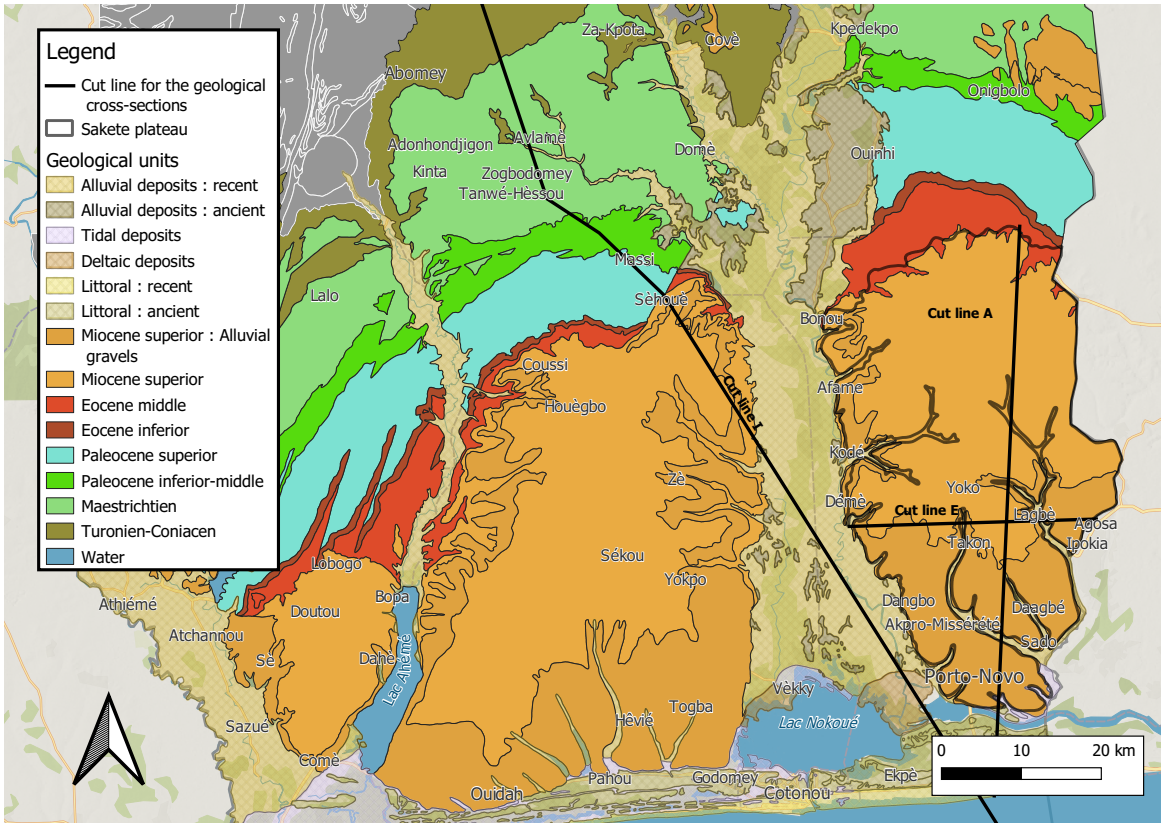

Figure 6: Map of the geology of the coastal sedimentary basin of Benin (Vincent and Hottin 1984)

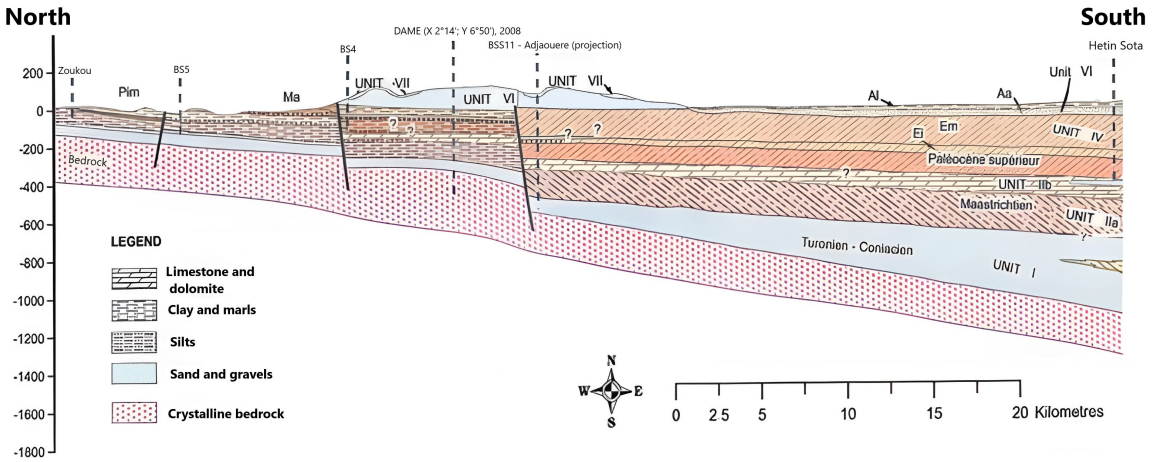

Figure 7: North-south geological cross-section of the coastal sedimentary basin of Benin, cut line I in Figure 6, note: the potential aquifers are represented in blue and the aquicludes in brown (modified from Achidi et al. 2012b)

The different geological units are defined by Achidi et al. 2012b as follows :

- Unit I - Turonian-Coniacian : sandy deposits, sandstone (siliceous or ferrous) with kaolin clay and gravels, directly on top of the bedrock. Thickness between 50 and 150m.

- Unit IIa - Maastrichtian : sands and quartzose sandstones with kaolin clays, transgressive on top of the Turonian-Coniacian. Maximum thickness $\simeq 180m$.
- Unit IIb - Lower Palaeocene : sands and quartzose sandstones with kaolin clays, with bioclastic oolitic limestone at the top of the unit. Thickness $\simeq 50m$.
- Unit III - Upper Paleocene / Lower Eocene : mainly clay with varying limestone content. Maximum thickness $\simeq 155m$.
- Unit IV Middle Eocene : clay base, then an alternation between decimetre thick limestone layers, kaoline clays and sandy clays. Thickness $\simeq 170m$.
- Unit V - Lower Miocene : limestone clays and sands. Thickness of at least $145m$ (the drilling that went through didn't reach its bottom).
- Unit VI - Upper Miocene : clayey sands, gravels and kaolin clays. It can be found in the meridional part of the plateaus, often altered in a ferric soil. Thickness $\simeq 120m$.
- Unit VII - Miocene-Pleistocene : gravels with a red clayey-sand matrix, found on top of the Miocene superior unit. Maximum thickness $\simeq 15m$.

The following figures (Figure 8 and Figure 9) show the geological structure of the Sakété plateau, according to A. Alassane 2004. The North-south inclination is clearly visible, and the piezometric levels can also be seen, in the "sand, gravel, sandstone and clayey sand" corresponding to the Mio-Pliocene aquifer and formations (units V, VI and VII).

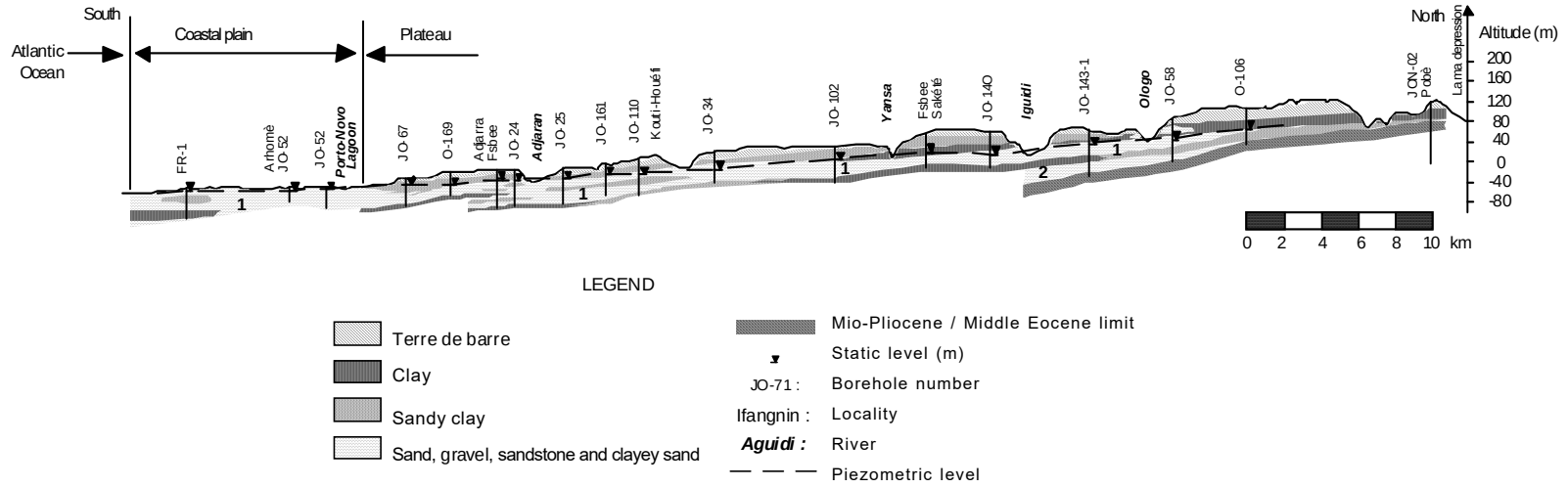

Figure 8: North-south geological cross-section of the Sakété plateau along the longitude 2°39'E, cut line A in Figure 6 (A. Alassane 2004)

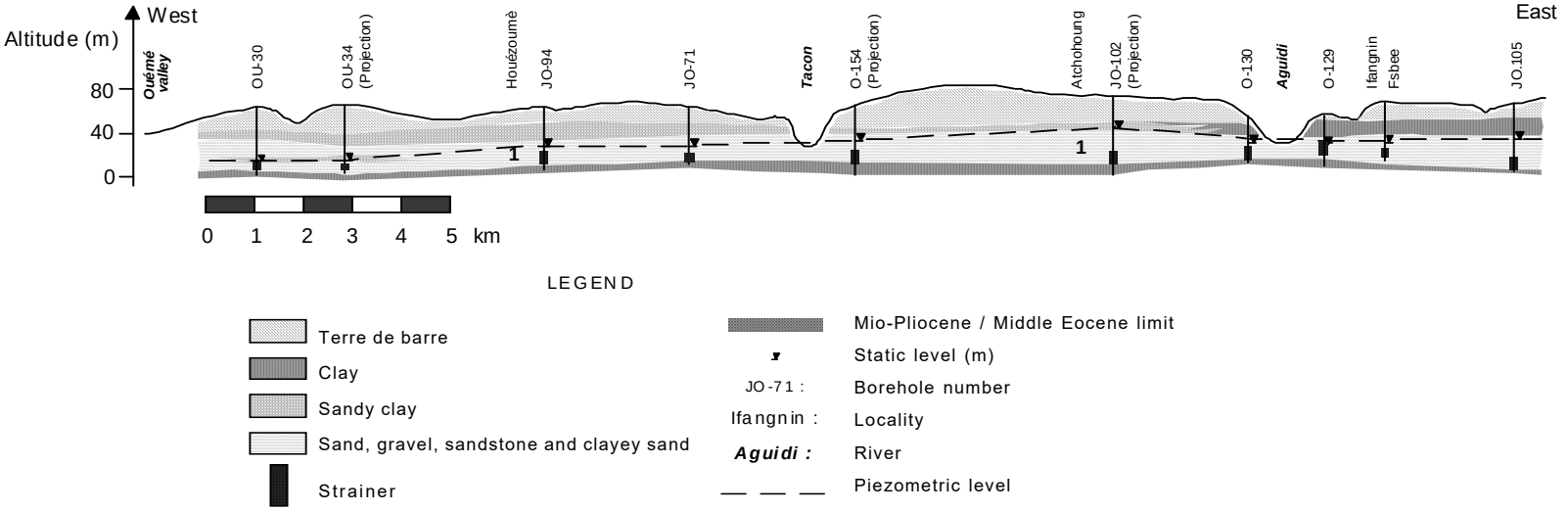

Figure 9: West-east geological cross-section of the Sakété plateau along the latitude 6°40'N, cut line E in Figure 6 (A. Alassane 2004)

2.8 Hydrogeology

The following table (Table 1) summarizes the different geological units and separates them regarding their hydrogeological properties (in terms of aquifer, aquitar and aquiclude).

Unit number	**Stratigraphic unit**	**Thickness (m)**	**Dominant lithology**	**Hydrogeological properties**	**Aquifer**
VII	Miocene-Pleistocene	$\simeq 15$	Fine sand	Aquifer	Mio-Pliocene aquifer[1]
VI	Upper Miocene	$\simeq 120$	Sand		
V	Lower Miocene	$\simeq 145$	Sand		
IV	Middle Eocene	$\simeq 170$	Marls	Aquiclude	Impermeable
III	Upper Palaeocene / Lower Eocene	$\simeq 155$	Clays and marls	Aquiclude	Impermeable
IIb	Lower Palaeocene	$\simeq 50$	Limestone and sand	Aquifer	Lower Palaeocene aquifer
IIa	Maastrichtian	$\simeq 180$	Clays and marls	Aquiclude	Impermeable
I	Turonian-Coniacian	$50 \sim 150$	Sand	Aquifer	Turonian-Coniacian aquifer

Table 1: Summary of the hydrogeological properties for the different units, from top to bottom (Kpegli 2020) ([1] Also called Continental Terminal aquifer in the literature)

The units VII to V, which encompass the Mio-pliocene aquifer, are the ones that were investigated. The majority of the waters that are pumped from the Sakété plateau comes from the Mio-pliocene aquifer, as the aquifer underneath (lower Paleocene aquifer) is located deeper, so it is necessary to dig deeper, which increases the cost of the installation of a drinking water point.

The piezometric levels of the study zone are presented in Figure 10. Coupled with the topography, the groundwater flow can be deduced : from north to south and from the centre of the plateau toward the west, in the Ouémé valley. This is clearly visible in the Figure 9, as the piezometric levels decrease toward the Ouémé valley.

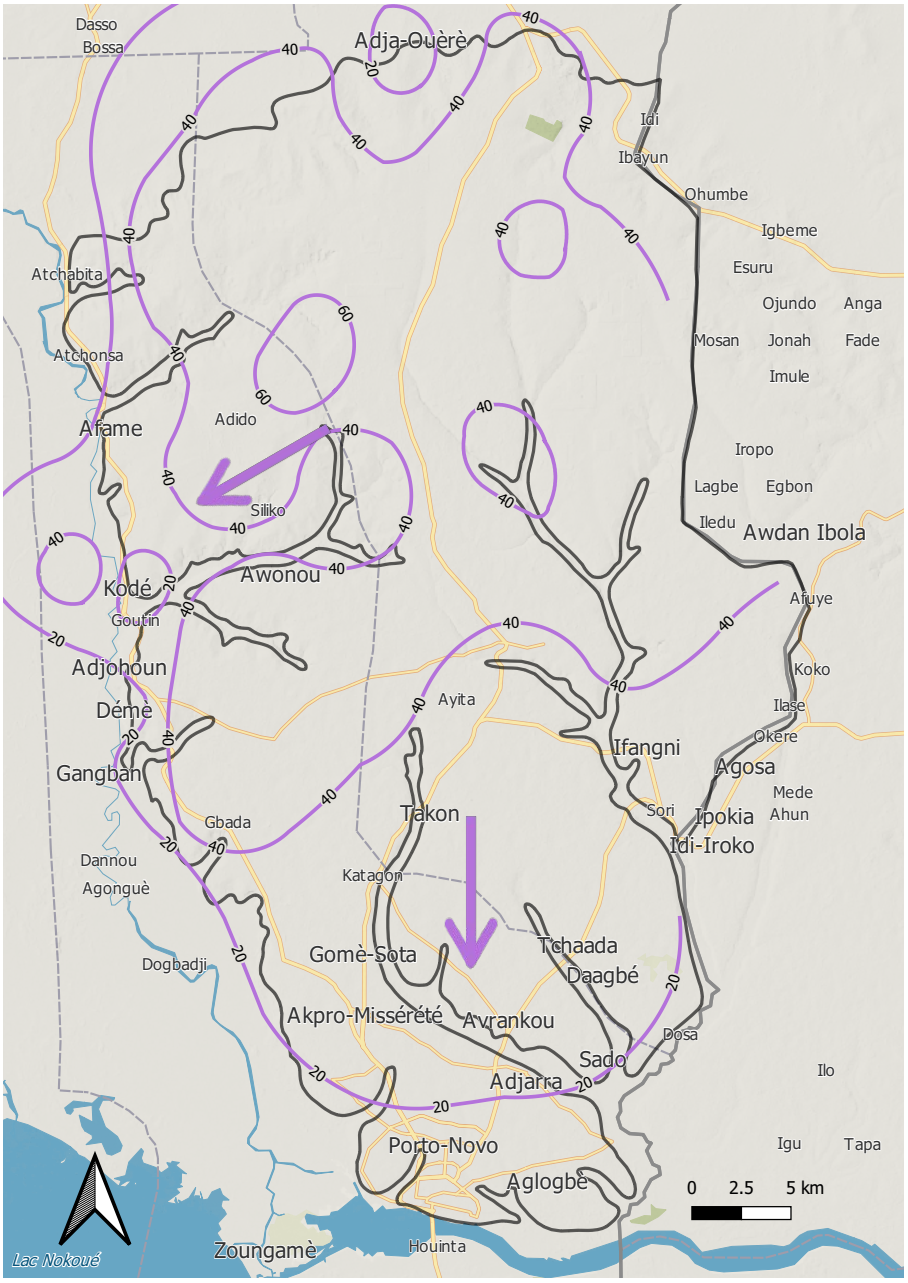

Figure 10: Map of the isopiezometric lines of the coastal sedimentary basin of Benin, the arrows representing the general groundwater flow (extracted from the Hydrogeological map of Bénin, Lucien et al. 2012)

The hydrogeological map of Benin (Figure 11) shows the potential for the exploitation of the groundwater (in a scale of blue to red), the lithology and the piezometric levels (in purple). The full legend of the map is available in the Appendix A.1.

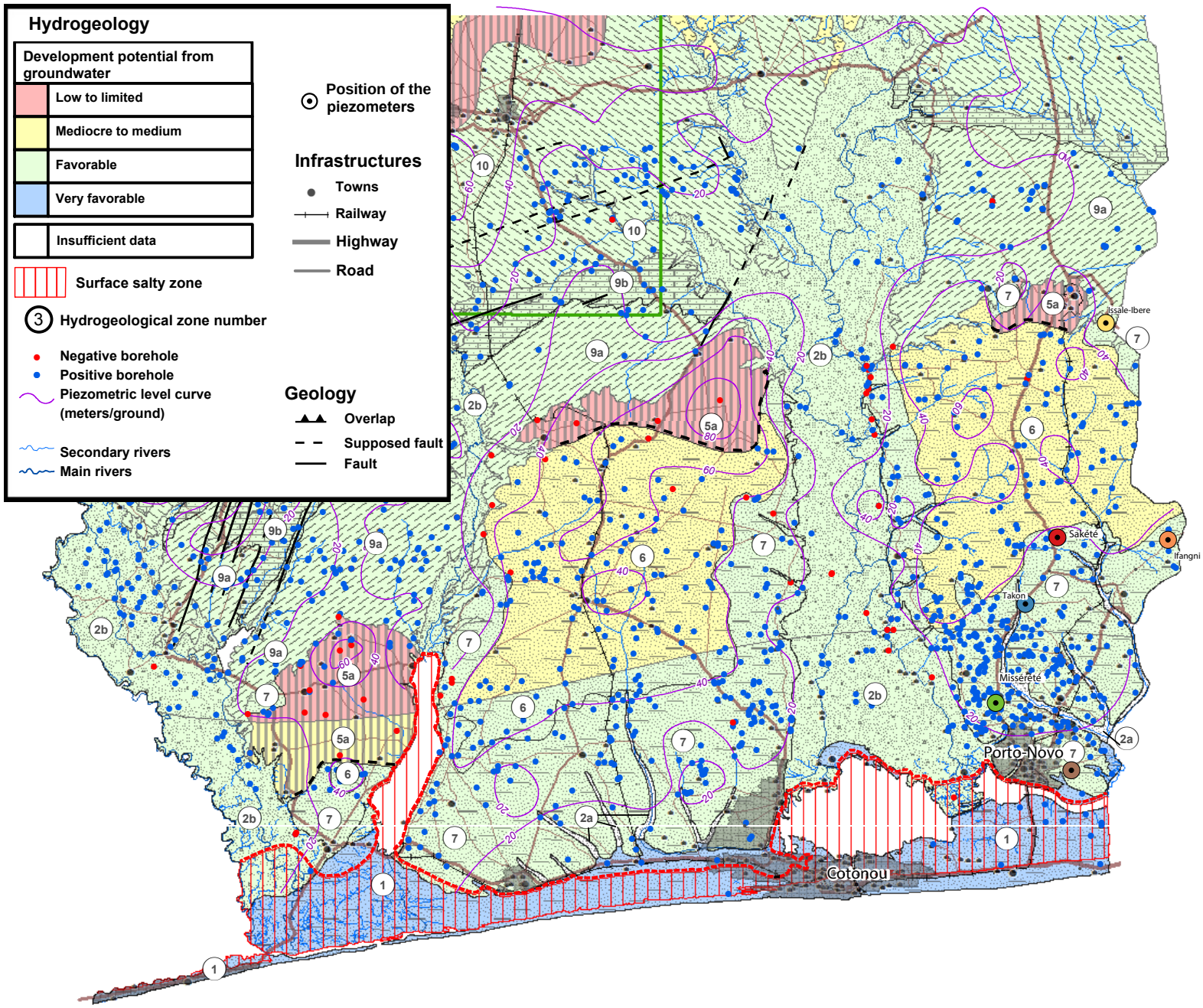

Figure 11: Hydrogeological map of Benin, cropped on the coastal sedimentary basin (Lucien et al. 2012)

3 Data collection and analysis

With the information collected in the previous section, a general idea of the hydrogeology of the region can be inferred. The Allada and Sakété plateaus are both formed from the same formations (units V to VII, dating from the Mio-Pliocene) and separated by the Ouémé River, which, by eroding these formations, separated these geographical units into two plateaus. Both plateaus are subjected to a great amount of precipitation due to the sub-equatorial climate with two rainy seasons, however the Sakété plateau receive on average more precipitation (from west to east, the mean annual precipitations increase from 900 to 1200 mm/year (Amoussou et al. 2016)).
The piezometric levels of both plateaus (visible in the Figure 11) are similar at the same distance from the sea, even with the Ouémé river separating the aquifers. This might indicate a link between both plateaus, which needs to be investigated to know if the conclusion concerning the water quantities of the Allada plateau can be extrapolated to the Sakété plateau.

To investigate the similarities between the Allada and Sakété plateaus, some data was needed. The data come from two sources : the majority of the data come from the internship that was carried with the DGEau and the INE in Benin, and the rest of the data were taken from the NASA POWER Project.
Three types of data were gathered during the internship : Magnetic Resonance Sounding (MRS), Time Domain Electromagnetic (TDEM) and water samples analysed later in Belgium for their ionic and isotopic compositions.

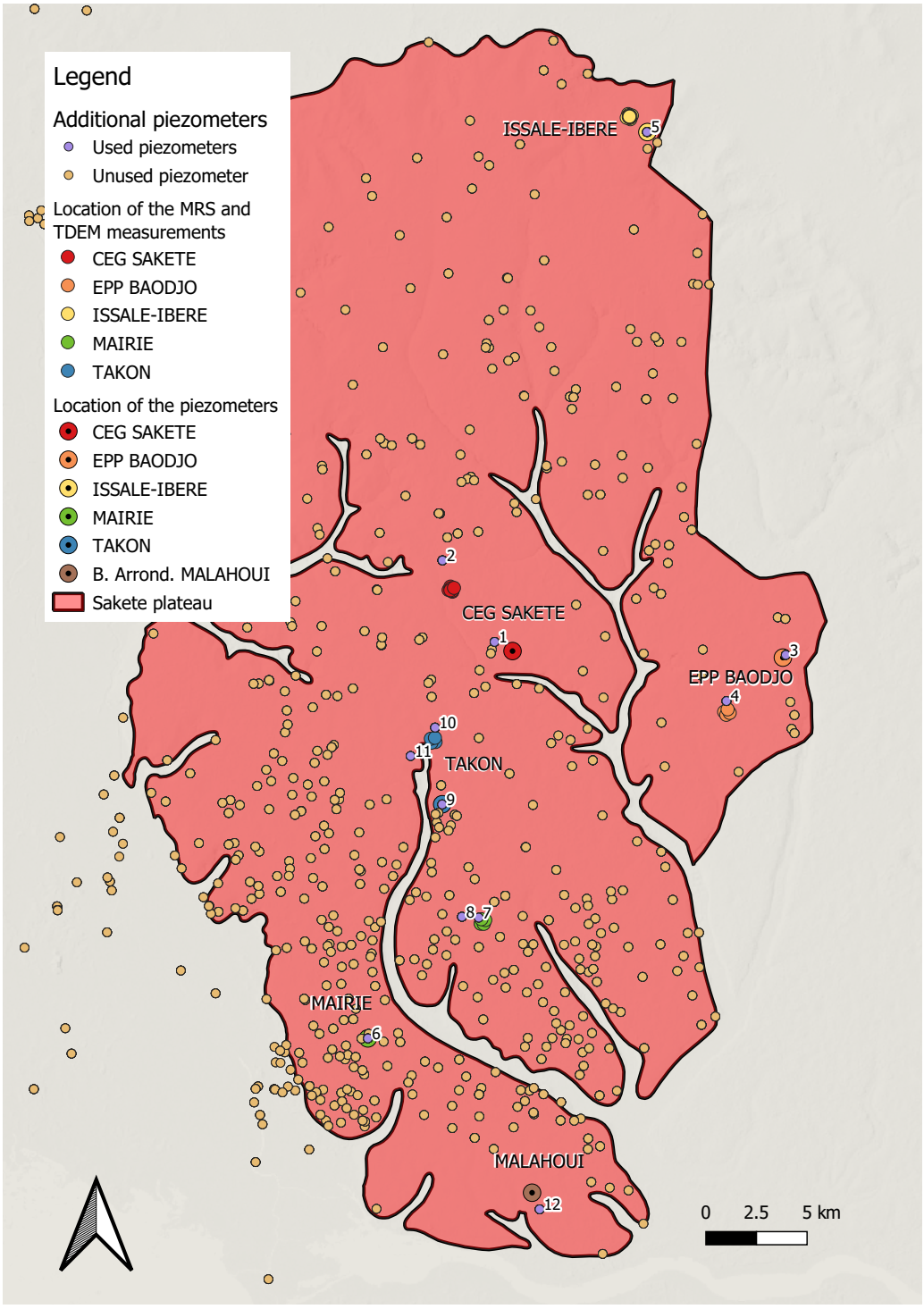

Figure 12: Location of the reference piezometers (where the water sample were taken), of the sites of MRS and TDEM measurements and of the additional piezometers of which the lithology is known

3.1 Geophysical surveys

Six piezometers belonging to the DGEau were chosen to represent the whole plateau, namely: "CEG SAKETE", "EPP BAODJO", "ISSALE-IBERE", "MAIRIE", "TAKON" and "MALAHOUI". The location of these reference piezometers can be found on the Figure 12, represented by colored circles with a dot. As they belong to the DGEau, it was possible to access them to get the piezometric level and to sample some water.

The locations chosen to perform the geophysical measurements were then determined on the basis of three main criteria:

- Proximity to the reference piezometer: the locations were chosen to be as close as possible to the 6 piezometers
- Practicability of the terrain: the location needed to be open spaces without too much bush or dense woods to be able to lay the loops without too much difficulty (and thus to avoid loosing time)
- Absence of a source of noise: each location was chosen to avoid as much as possible dwellings (most of which have sheet metal roofs and generators, both a source of noise) and high voltage lines to avoid the noise as much as possible

The location of these measurements sites can be found on the Figure 12, represented by colored circles. However, for the site MALAHOUI, the piezometer was located too close to Porto-Novo, so the anthropic noise was too high to conduct any measurements, so only 5 locations were investigated. This map also shows the distribution of known piezometers on the Sakété plateau (orange dots), of which some information are known (total depth, lithology and main hydrological unit).

As the lithology of some of the 6 piezometers was not properly recorded when the drillings were conducted, the information from the other piezometers were used. The piezometers that were used were chosen as close to the measurement sites as possible, and are shown as violet points with a number on the Figure 12, and were used to correlate the geophysical results and the actual underground.
The lithology for each used additional piezometers can be found in the Appendix A.2.

3.1.1 MRS

Magnetic Resonance Sounding (MRS) is a geophysical technique that differs from the other techniques in that it can unequivocally detect groundwater, as it measures a signal that comes directly from the excitation of the hydrogen nuclei ($^1H^+$), which correlates to the free water content. The signal decay rate can also be linked to the porosity of the medium, giving another information regarding the hydrogeological parameters of the underground.

The hydrogen nuclei have a weak nuclear magnetic moment and are thus, on average, aligned with the local magnetic field. In the absence of stimulation, it will be aligned with the terrestrial magnetic field. By creating a magnetic field using a current I for a time τ (the product $I\tau$

being called the excitation moment Q, in A·ms) in a loop above ground, the hydrogen nuclei will align with the new magnetic field, and when the magnetic field stops, they will leave their excited phase to realign with the original magnetic field, creating an alternating magnetic field oscillating at the Larmor frequency of the hydrogen nuclei ($^1H^+$), which induces an alternating voltage in the measuring loop. The measured voltage depends on the excitation moment Q, the quantity of free water in the subsurface and its depth, the subsurface conductivity, the loop size and shape and the local value of the Earth's magnetic field (Roy and Lubczynski 2003).
As the hydrogen nuclei leave an excited phase to reach a more stable one, the measured relaxation signal will be a decreasing curve, called the relaxation curve.
The pore size of the medium is proportional to the slope of the relaxation curve (or decay rate), and the initial T_2^* value is proportional to the water content.

By repeating the measure for different values of Q, it is possible to know the depth of the measured water content as the measured response for a small value Q is linked to the water near the surface, whereas for larger values of Q the deeper water will have a significant impact on the measured response (Roy and Lubczynski 2003).

3.1.1.1 Acquisition of the data

The data was acquired using the Numis Poly from IRIS Instruments. The location chosen for the measurements is "CEG SAKETE", the same as the one chosen for the TDEM measurements.

The acquisition settings are as follows:

- Square loop of 125x125m, 1 turn
- Larmor frequency of 1400 Hz
- Stacking under the maximum noise level of 2000 nV, with 700 stacks (or less if the data curve is well separated from the noise)
- Geomagnetic field : 32863.85 nT
- Pulse parameter :
  - Noise acquisition time : 240 ms
  - Double pulse T_2^* and T_1, both with a pulse duration of 40 ms and a recording time of 240 ms
  - Delay between the pulses : 15 ms
  - Dead time of 40 ms

3.1.1.2 Quality of the data

Although the acquired data has a good quality, i.e. a high signal over noise ratio, as can be seen in Figure 13, only one location has been investigated due to a lack of time and a national shortage of fuel.
Due to faulty batteries, no pulse higher than 9116.9 A.ms could be injected, but the beginning

of the decline of the curve, which is used to determine the porosity of the medium, can still be observed.

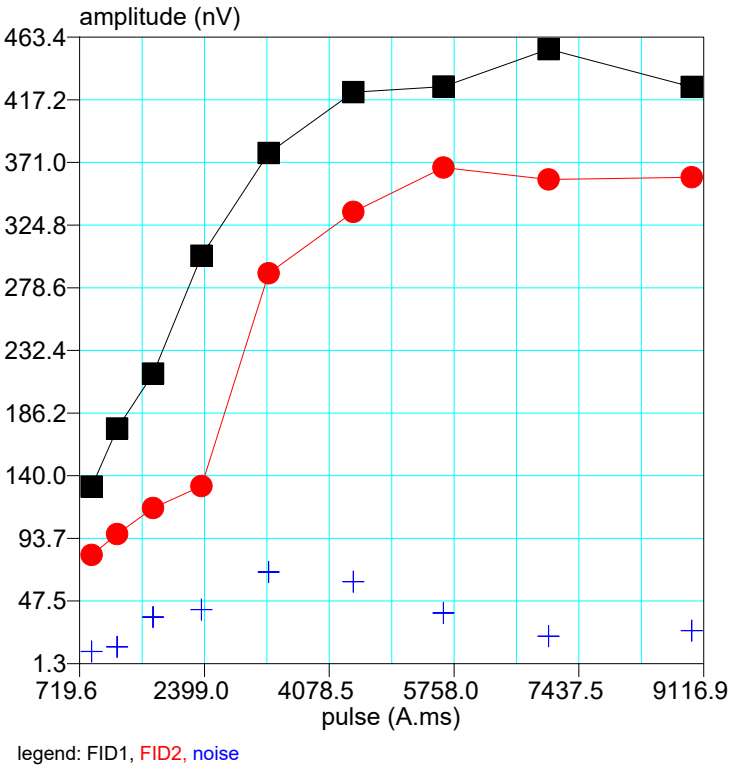

Figure 13: Evolution of the mean of the measured signals (FID1, FID2 and noise), depending on the value of the injection pulse Q

3.1.1.3 Inversion parameters

The software used to compute the inversion is the free software SAMOVAR 6x7, that can conduct the inverse modelling of MRS data and is fully compatible with data from the Numis Poly of IRIS Instruments.
To unsure that the comparison with the results obtained on the Allada plateau is valid, a similar inversion method was used : the signal processing is done with a bandpass filter of 10 Hz, and the inversion parameters are left for the software to compute. The start model is the default one, one layer 300 m thick with a resistivity of 300 $\Omega.m$. The summary of the inversion parameters used by the software is as follows :

```
loop: square, side = 125.0 m
geomagnetic field: inclination = 15 degree, magnitude = 32863.85 nT

filtering window = 197.1 ms
bandpass = 10.00 Hz
permeability constant Cp = 7.00e-09

average signal to noise ratio (S/N) = 8.47;
external noise to the internal noise ratio (EN/IN) = 8.09
mean noise = 23.74 nV
fitting error:
    RMSE FID1 = 25.82 nV
    RMSE FID2 = 42.42 nV
    RMSE T1 = 123.74 ms
parameter of regularization (PR)
    PR w = 750.0
    PR T1 = 690.460
number of layers = 9
number of pulse moments = 9
```

The computed average signal over noise ratio of 8.47 confirms the good quality of the data, and the fitting error (25.82 and 42.42 nV) being in the same value range as the mean noise (23.74 nV) indicates a good fit.

3.1.1.4 Results of the inversion

The Figure 14 shows all the measured relaxation curves and the exponential fits made by the inversion of the data set and the Figure 15 shows a zoom on one of the curves, where the relaxation curve is more visible.

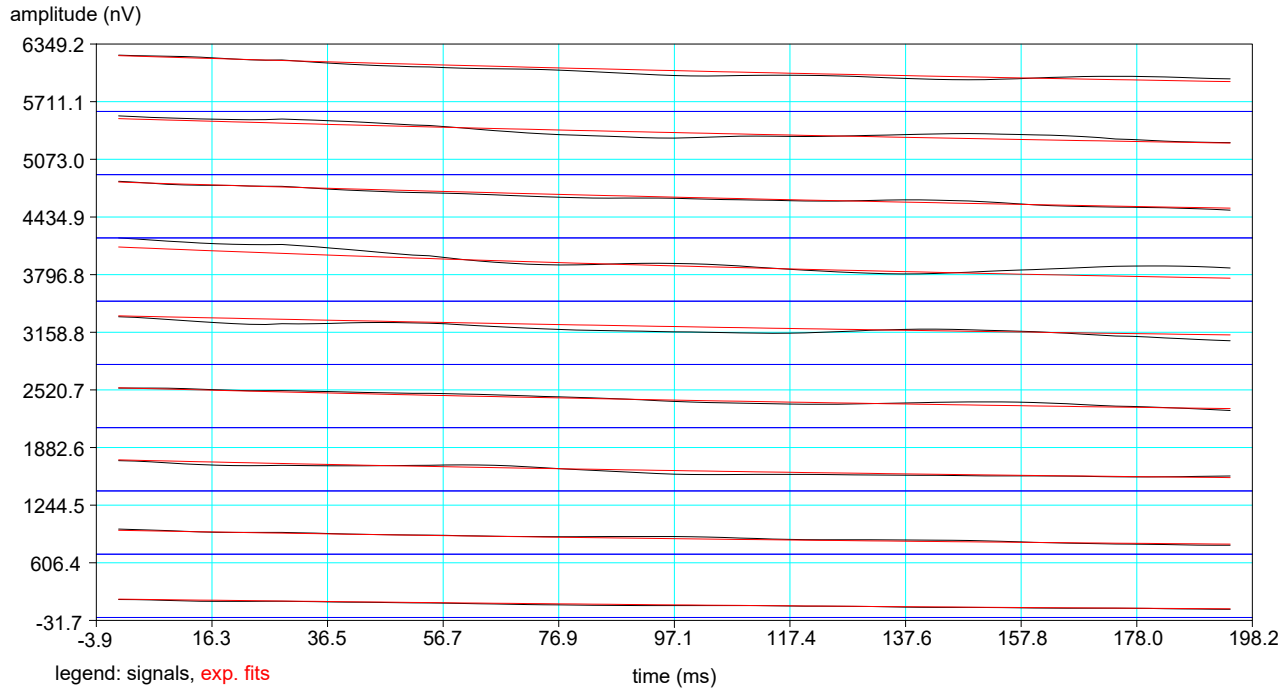

Figure 14: Measured relaxation curves (black) and exponential fits (red) for the data set

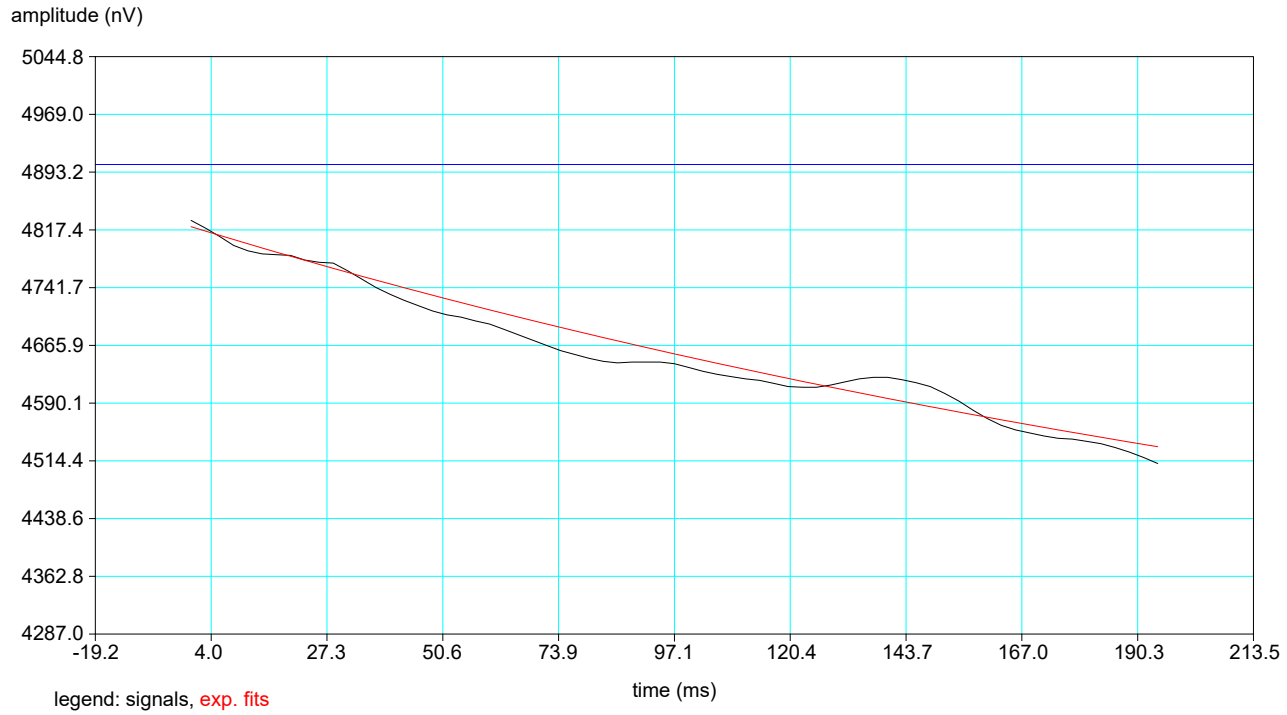

Figure 15: Zoom on one of the measured relaxation curve (black) and its exponential fit (red) of the data set

The inversion result (Figure 16) shows that there is a really small water content (less than 2%) in the first 20 m, then a higher water content can be observed past 40 m, with a pike (of about 22%) in water content near 80 m, and further down a slightly lower water content (about 15%).

The Figure 17 shows the evolution of the relaxation time T_1 along the depth, and the correlation between this relaxation time and the water content can be seen by comparing both figures. For a given depth, a high value of T_1 corresponds to a high water content.

The depth also influences the link between both variables, as the signal decreases with the depth. This means that for a given T_1, the depth and water content are proportionate.

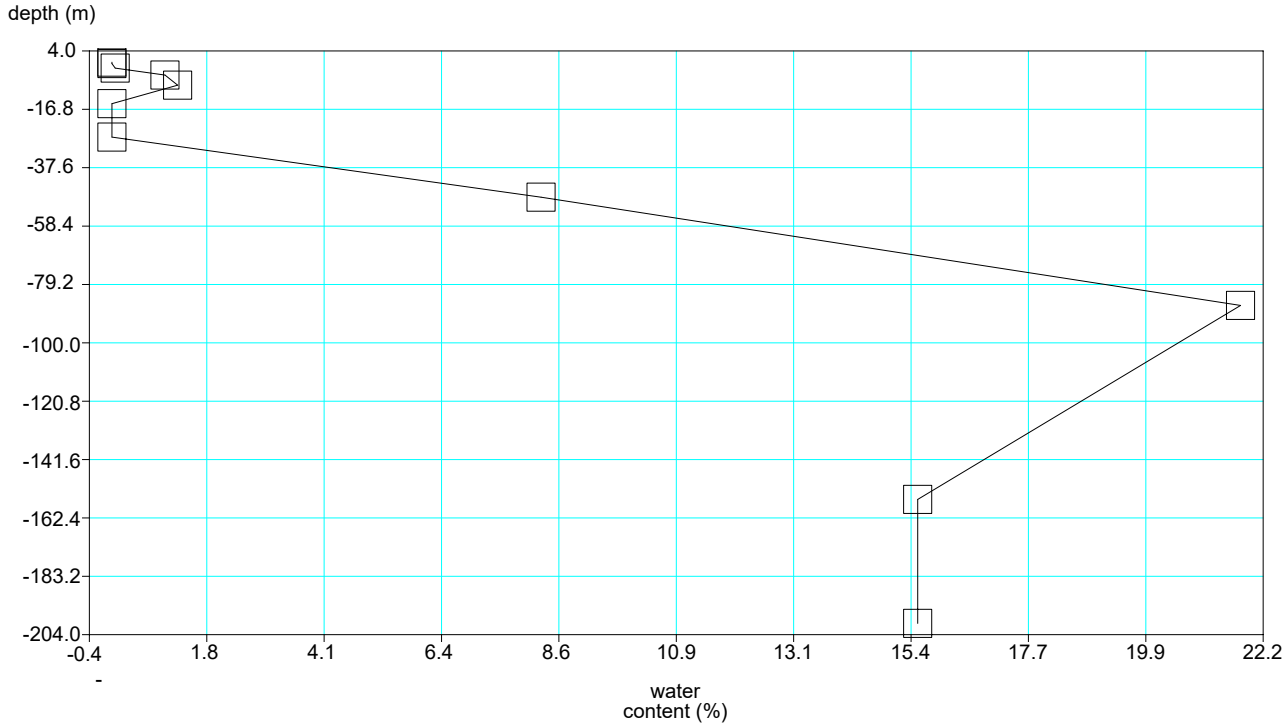

Figure 16: Evolution of the water content along the depth (result of the inversion)

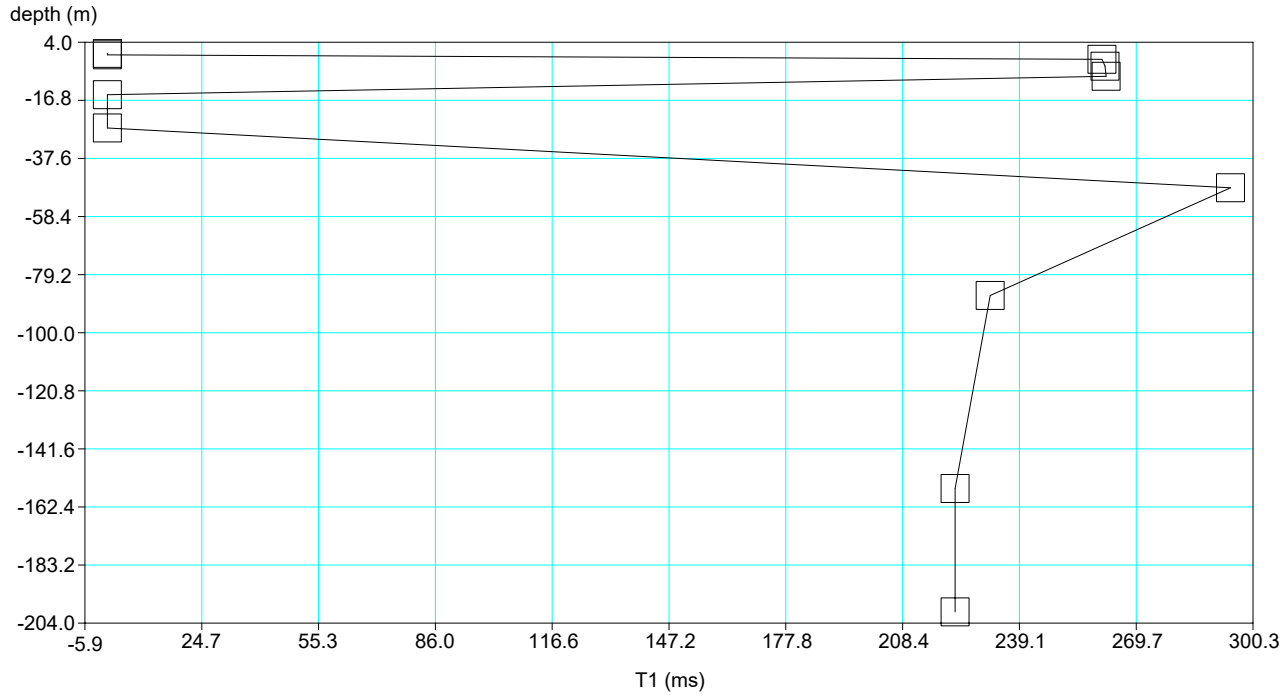

Figure 17: Evolution of the relaxation time T_1 along the depth

Finally, the Figure 18 shows the interpretation results of the software SAMOVAR. The main aquifer appears to be situated under 60 m, with the region between 37 and 59 m having a smaller water content. This result is coherent with the hydrogeological cross-section in Figure 9, which shows a piezometric level around the 40 m depth mark, underneath a sandy clay layer topped with a Terre de barre layer.

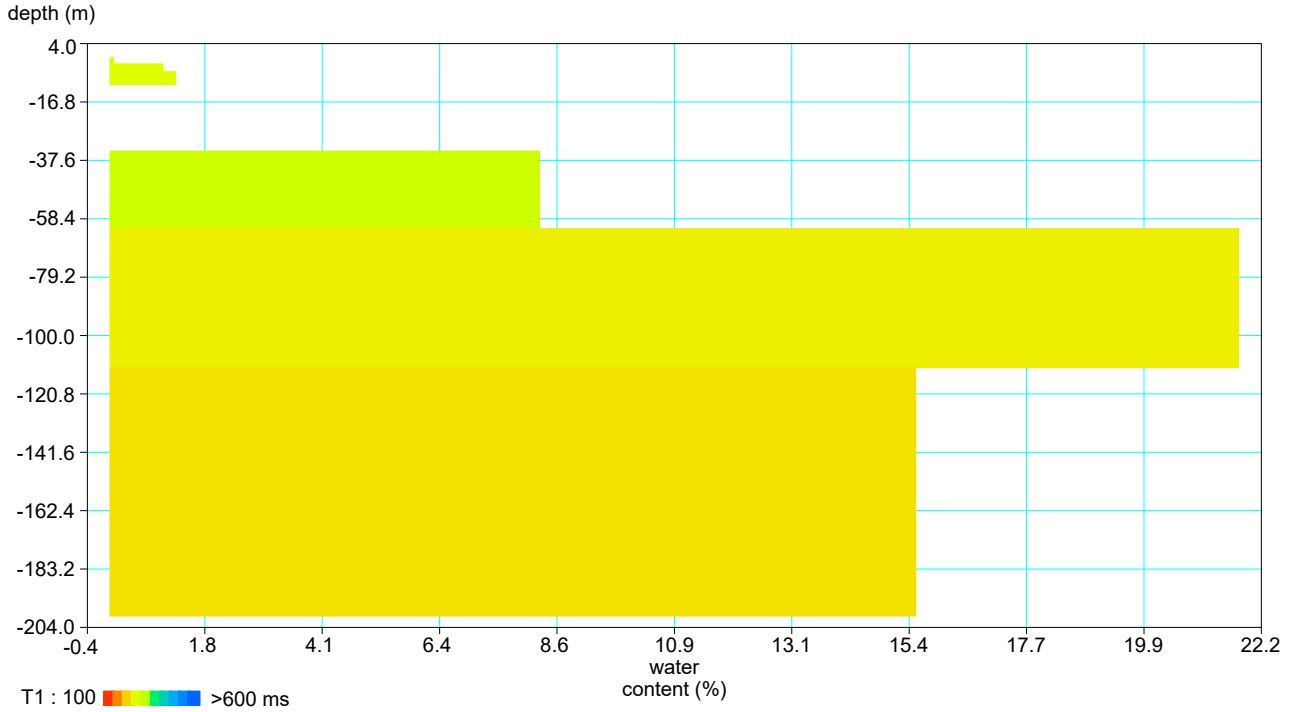

Figure 18: SAMOVAR interpretation results for water content, with the color scale representing the relaxation time T_1 (in ms), along the depth (in m)

3.1.1.5 Conclusion from the method concerning the water content of the site

Looking at the result obtained from the inversion in Figure 18, it is possible to have an approximation of the depth of the piezometric level and the general geometry of the aquifer:
First, there is almost no water content in the 37 first meters (`zone A`). Then, 3 zones can be defined: one from 37 to 59 m depth (`zone B`) with a water content of about 8.4%, one from 59 to 110 m (`zone C`) with a water content of about 22.2%, and one from 110 m to 200 m (`zone D`) with a water content of about 15.8%. The first signs of water being around 37 m depth is coherent with the piezometric levels presented in Figure 10, the point of measurement being near the 40 m isopiezometric line.

Using the lithological data from the nearest drilling (Table 9 in the Appendix A.2), it can be seen that the first small water content from the `zone A` is some water trapped above a clay layer situated between 12 and 23 m depth. The `zone B` is situated in coarse to medium sand, the `zone C` is in medium to fine sand. There is no information further than 90.7m on this drilling, so the `zone D` porous medium isn't known with certainty.
However, comparing the inversion results with the lithology of the region (Table 1) gives another information: it appears that the wet layer (`zone B` to `zone D`) corresponds to the Mio-Pliocene aquifer, which is the one that was expected. In theory, this aquifer, composed of the stratigraphic units VII (Miocene-Pleistocene), VI (Upper Miocene) and V (Lower Miocene), has a

thickness of about 280 m. The inversion result has a maximum depth of 200 m, so it is coherent that the impermeable marl layer situated underneath the sandy aquifer doesn't appear on the inversion.

3.1.2 TDEM

Time-domain electromagnetic (TDEM) is a geophysical technique based on the response of the subsurface to an electromagnetic field. This primary electromagnetic field is a series of pulse generated by injecting an alternating current into a square loop above ground, which induces a secondary Eddy current in the conductors present in the subsurface, which in turn induces a secondary electromagnetic field.
The secondary field is then measured in a concentric receiving loop by the alternating currents induced by the secondary electromagnetic field. The measurement is conducted when the primary one is absent because the primary field has a much larger amplitude than the secondary field (Kearey, Brooks, and Hill 2002).
By repeating the measurement for longer and longer periods of time, it is possible to obtain information on greater and greater depths. This measurement gives a 1D image that represents the subsurface under the loop.

3.1.2.1 Acquisition of the data

The data were acquired using the ABEM WalkTEM from Guideline Geo. The measurements were conducted on the 5 sites that were chosen for their proximity to the reference piezometer wells (Figure 12) and their relatively isolated location, to avoid as much as possible the anthropogenic noise.

The ABEM WalkTEM comes with a set of scripts for the measurement that are useful for different situations. To choose which script to use, on the first investigated site (ISSALE-IBERE), measurements were carried out with different protocols available, then the results were assessed visually to determine the protocol that gave the best results.

The WalkTEM User's Guide (ABEM 2016) describes the different scripts as follows :

- DualMoment_30ms_40gates 50Hz: Measuring script for shallow to deep data collecting when a longer measuring time is required, divided into 40 gates
- HighMoment_Noise_10_90ms_51gates 50Hz: Measuring script for very deep data collecting, divided into 51 gates
- DualMoment_Testscript 50Hz: Fast measuring script, equal number of High, Low and Noise moment measurements. Useful for quick tests of equipment and measuring site.
- DualMoment_10ms_40gates 50Hz: Measuring script for shallow to deep data collecting, divided into 40 gates

The "Dual Moment" (DM) is a combination of low moments (LM) and high moments (HM). The LM can get information on the shallow part of the subsurface, while the HM can get information at higher depth (Neven et al. 2021).

The "gate" is the time period on which the signals are received and averaged, and as the signal decreases with passing time, the gate size grows along the measure.

After a visual inspection, the protocol that was chosen is the "DualMoment_30ms_40gates" as the results are the ones that gave the best signal over noise ratio and a curve without too many oscillations. The following figures (19, 20 and 21) show the curves obtained from the different DM scripts, as they had less noise than the HM. The Figure 19 has too much noise, and the Figure 20 is used to conduct a quick measuring for equipment and site testing. The script used in Figure 21 is thus the one that is used for the further measurements.
In this script, the duration of the gates ranges from 2 to 6070 μs, for a total measuring time of 29514 μs (which corresponds to the "30ms").
Another advantage of this measure is that it has a duty cycle of 25%, which can decrease the heat load on the WalkTEM, as specified in the WalkTEM user manual (ABEM 2016) when working in hot conditions.

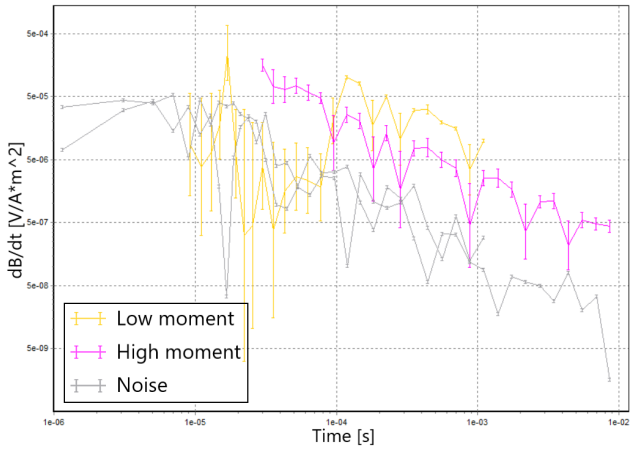

Figure 19: First site (ISSALE-IBERE), station n°6, protocol used: DualMoment_10ms_40gates, evolution of the stacked dB/dt data and noise (in V/Am^2) over time (in s)

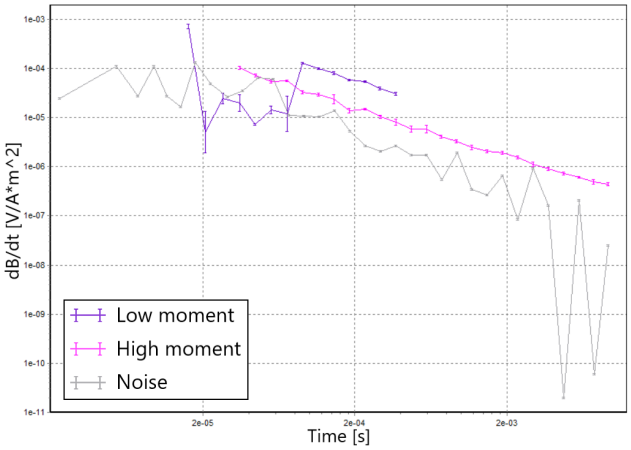

Figure 20: First site (ISSALE-IBERE), station n°5, protocol used: DualMoment_Testscript, evolution of the stacked dB/dt data and noise (in V/Am^2) over time (in s)

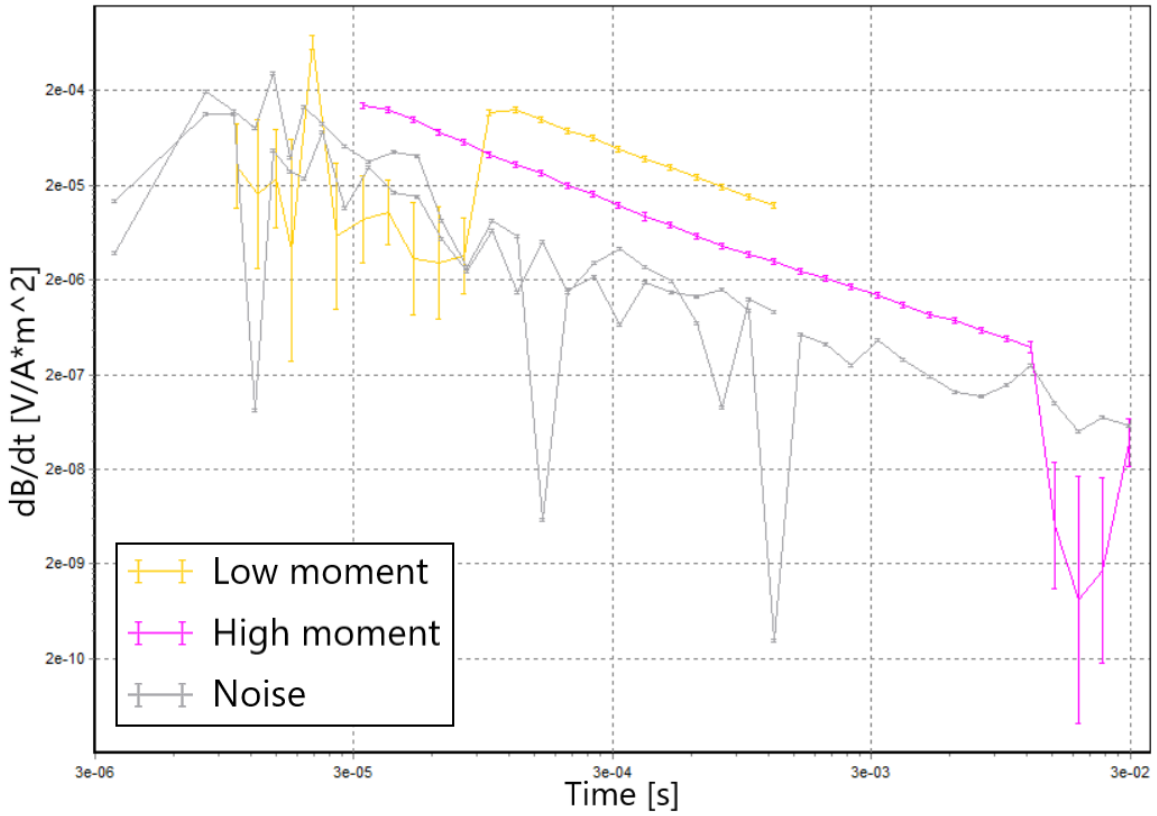

Figure 21: First site (ISSALE-IBERE), 200x200m loop, protocol used: DualMoment_30ms_40gates (chosen script), evolution of the stacked dB/dt data and noise (in V/Am^2) over time (in s)

3.1.2.2 Quality of the data

The data obtained on the different sites have variable levels of noise. The following figures (22 and 23) show the variability in the quality of the data. Some appear extremely good (a smooth curve above the noise level, Figure 22), while others are impossible to interpret as the noise is too strong (less than 6 points above the noise level and an extremely noisy curve, Figure 23).

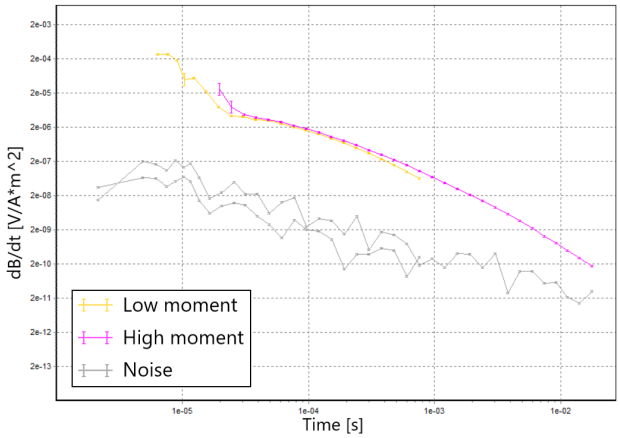

Figure 22: Example of good data quality : site MAIRIE, 200x200m loop, evolution of the stacked dB/dt data and noise (in V/Am^2) over time (in s)

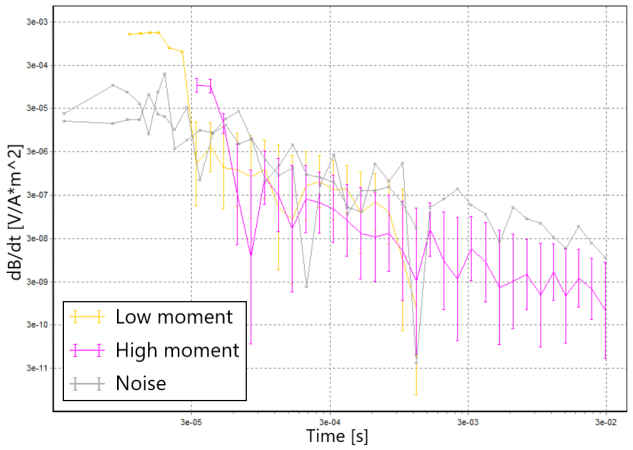

Figure 23: Example of bad quality : site SAKETE, 200x200m loop, evolution of the stacked dB/dt data and noise (in V/Am^2) over time (in s)

Of the 5 locations where measurements were made, SAKETE and TAKON had too much noise for the interpretation to be possible.

3.1.2.3 Data processing and inversion

The display and inversion of the obtained data was carried with the software SPIA TEM, version 3.2.0.0. It is compatible with the data from the ABEM WalkTem, automatically filters the noise and the spikes, and allows the user to select the data used for the inversion directly on the plots.

The data were first analysed to find dB/dt curves without too many sudden fluctuations and where the low moment curve overlaps with the high moment curve, according to the SPIA TEM manual (Aarhus GeoSoftware 2022).

For the 3 locations that didn't appear too much impacted by noise, one inversion was done for the data curve that appeared the smoother and with the less noise. The data were then trimmed to remove the sudden fluctuations and the areas where the noise have too much influence (i.e. where the data curves meets the noise curves). This is represented for the three data sets that were selected in the following figures (24, 25 and 26):

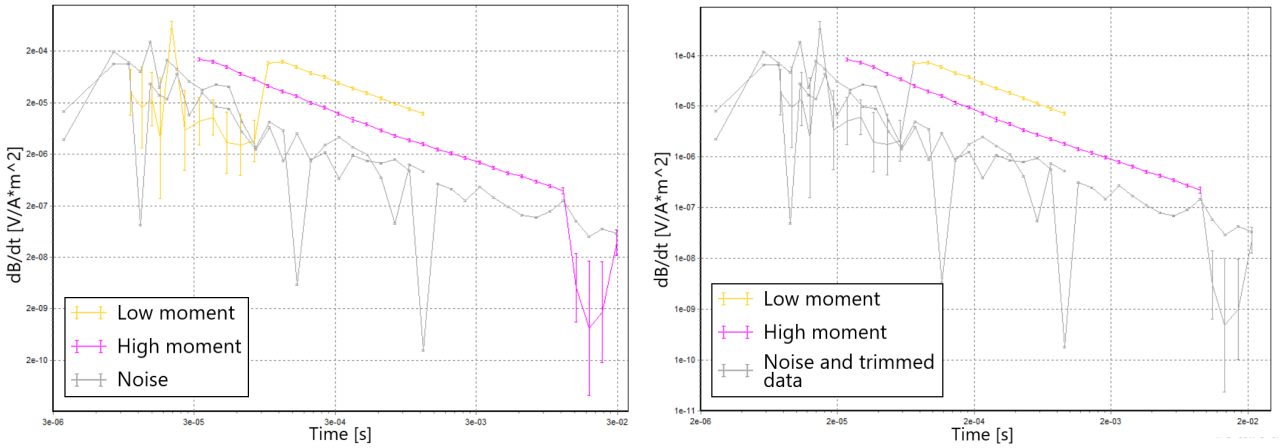

Figure 24: Site ISSALE-IBERE, 200x200 m loop, evolution of the stacked dB/dt data and noise (in V/Am^2) over time (in s), original (left) and trimmed (right) data set

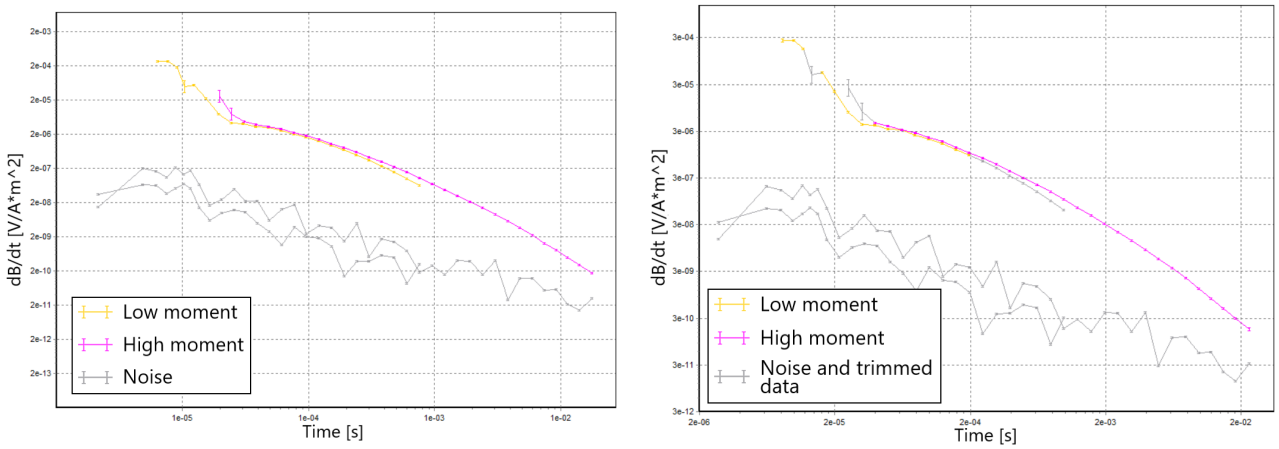

Figure 25: Site MAIRIE, 200x200 m loop, evolution of the stacked dB/dt data and noise (in V/Am^2) over time (in s), original (left) and trimmed (right) data set

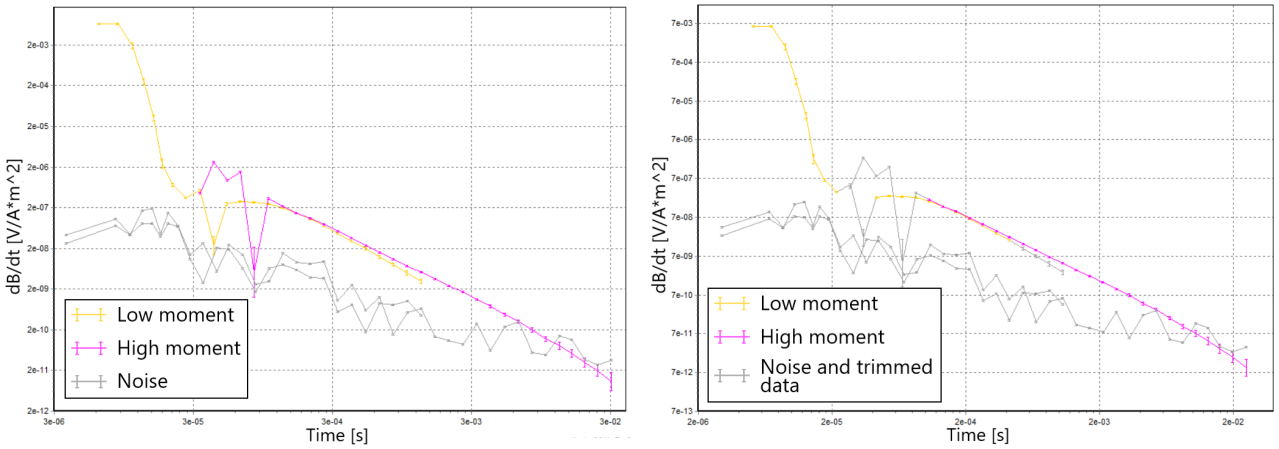

Figure 26: Site EPP BAODJO, 40x40m loop, evolution of the stacked dB/dt data and noise (in V/Am^2) over time (in s), original (left) and trimmed (right) data set

It is interesting to note that for the site EPP BAODJO, the best curve was obtained on the smallest loop (40x40 m). This seems strange because a bigger loop will get more information and thus should have a better signal over noise ratio. The reason for this can be linked to the temperature that increases over time inside the WalkTEM. Indeed, over time heat accumulates inside the WalkTEM as it function, but the outside temperature also increases as the first measures were taken in the morning, when the ambient temperature was lower.

3.1.2.4 Results of the inversion

The inversion of the three data sets are presented in the following figures and tables: Figure 27 and Table 2 for the site ISSALE-IBERE, Figure 28 and Table 3 for the site MAIRIE, Figure 29 and Table 4 for the site EPP BAODJO.

On the first inversion results, for the data from ISSALE-IBERE (Figure 27 and Table 2), the fitted curve does not follow the data, which can be seen with the high standard deviations (STD) in terms of resistivity and layer thickness. Thus, the model won't be interpreted.

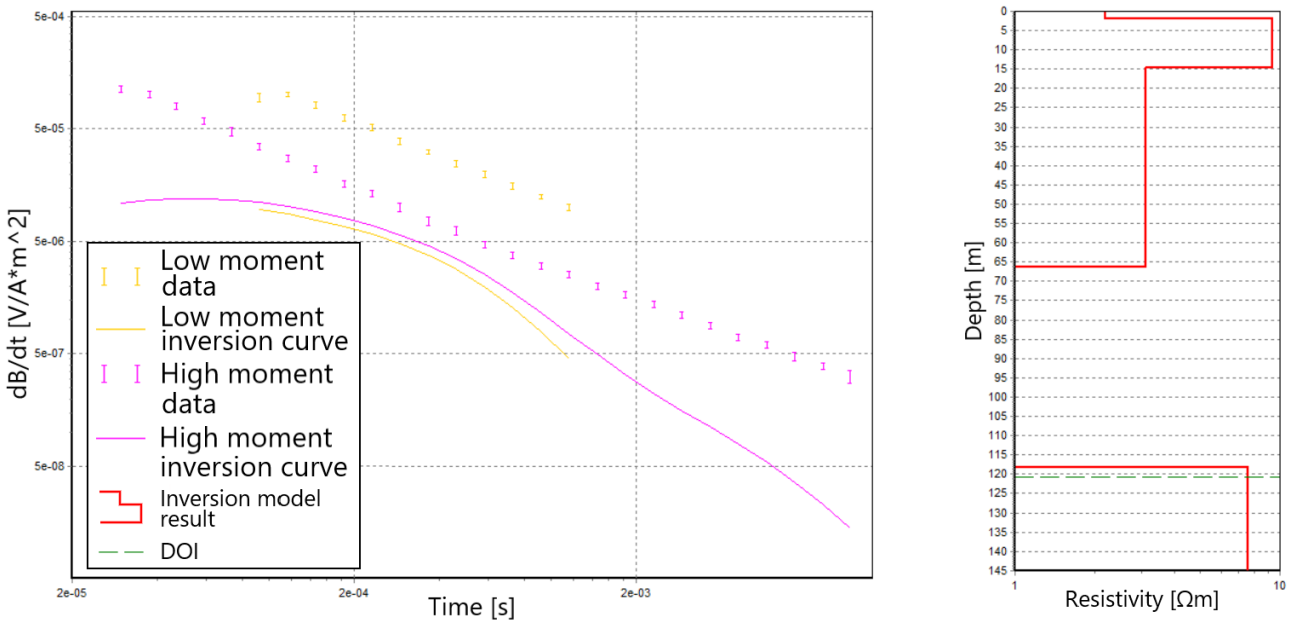

Figure 27: Site ISSALE-IBERE, result of the inversion. Left: Evolution of the stacked dB/dt data and fitted inversion curves (in V/Am^2) over time (in s), right: Inversion model result and DOI (DOI of 121 m)

Layer	Resistivity $[\Omega.m]$	Resistivity STD $[\Omega.m]$	Thickness $[m]$	Thickness STD $[m]$	Depth $[m]$	Depth STD $[m]$
1	2.19	99.00	1.88	99.000	1.88	99.000
2	9.41	99.00	12.7	99.000	14.5	2.740
3	3.13	1.13	51.9	1.558	66.4	1.618
4	0.711	1.29	51.7	1.829	118	1.101
5	7.57	99.00				

Table 2: Numerical inversion results for the site ISSALE-IBERE

Contrary to the previous inversion, the inversion of the data from the sites MAIRIE and EPP BAODJO shows fitted inversion curves that follow the data trend (Figure 28 and Figure 29), with only a high uncertainty on the resistivity for one layer each (Table 3 and Table 4), corresponding to a high resistivity. This was expected for these high values, as according to the SPIA TEM manual (GeoSoftware 2022): "The TEM method has a poor resolution when determining the exact resistivity of a layer with high resistivity, and a layer with a resistivity of 1000 $\Omega.m$ has almost the exact same response as a layer with a resistivity of 100 $\Omega.m$".

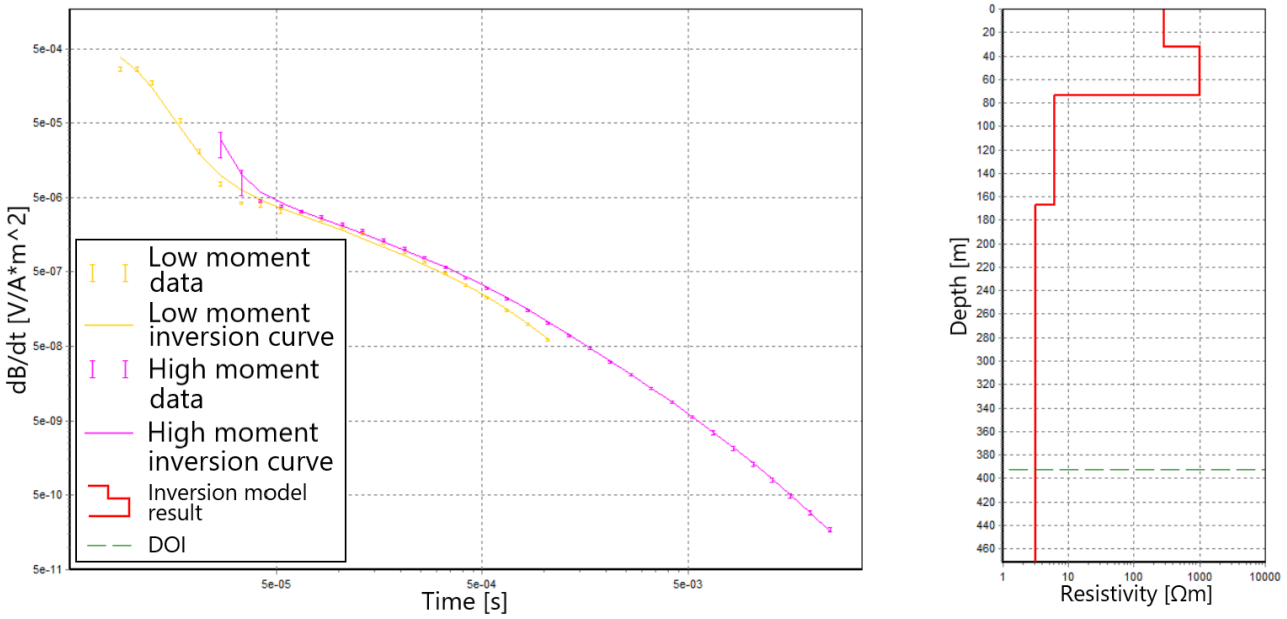

Figure 28: Site MAIRIE, result of the inversion. Left: Evolution of the stacked dB/dt data and fitted inversion curves (in V/Am^2) over time (in s), right: Inversion model result and DOI (DOI of 393m)

Layer	Resistivity $[\Omega.m]$	Resistivity STD $[\Omega.m]$	Thickness $[m]$	Thickness STD $[m]$	Depth $[m]$	Depth STD $[m]$
1	287	1.11	32.7	2.29	32.7	2.29
2	1030	99	40.8	2.13	73.5	1.051
3	6.19	1.02	93.7	1.066	167	1.06
4	3.18	1.07				

Table 3: Numerical inversion results for the site MAIRIE

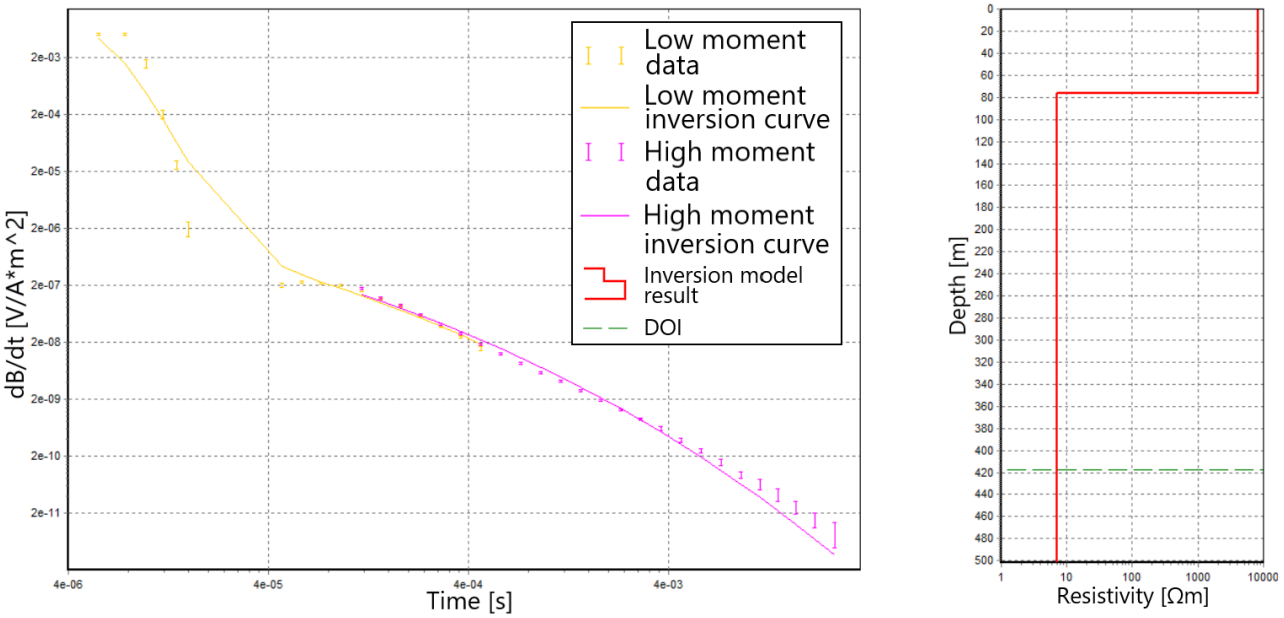

Figure 29: Site EPP BAODJO, result of the inversion. Left: Evolution of the stacked dB/dt data and fitted inversion curves (in V/Am^2) over time (in s), right: Inversion model result and DOI (DOI of 418m)

Layer	Resistivity $[\Omega.m]$	Resistivity STD $[\Omega.m]$	Thickness $[m]$	Thickness STD $[m]$	Depth $[m]$	Depth STD $[m]$
1	1.1	4.05	0.159	4.210	0.159	4.210
2	8370	99.00	75.8	1.020	76	1.017
3	7.12	1.03				

Table 4: Numerical inversion results for the site EPP BAODJO

3.1.2.5 Conclusion on the geology/hydrogeology of the sites

By comparing the computed resistivities with the lithological data from nearby drillings (Table 13, Table 14 and Table 15 for MAIRIE and Table 10 and Table 11 for EPP BAODJO, in the Appendix A.2), it is possible to correlate the computed resistivity to the expected lithology and thus to know if the water is present.

For the site MAIRIE, the lithology and estimated water content for each layer is as follows:

- Layer 1: Mainly sandy clay on top of a medium sand, probably with very little water content, which explains the resistivity around $300\Omega.m$.
- Layer 2: Mainly sand with some clay, the high resistivity around $1000\Omega.m$ implying a dry medium.
- Layer 3: No more information is known from the drillings, but the lithology of the region (Table 1) suggest that the main lithology is still sand. The low resistivity (around $6\Omega.m$) shows that the medium is wet.

- Layer 4: Same as the previous layer, the lithology might still be sand. However, the even lower resistivity value (around 3 $\Omega.m$) might be linked either to a high clay content (which could indicate that the Middle Eocene layer has been reached) or that there is some more conductive water coming from the Lower Palaeocene aquifer that is situated underneath.

For the site EPP BAODJO, the lithology and estimated water content for each layer is as follows:

- Layer 1: Mainly clayey sand, the very low resistivity of 1 $\Omega.m$ suggests that this is mostly clay. This layer, however, is very thin (about 0.1 m thick) and can thus be linked to an error linked to the inversion.
- Layer 2: Mainly clay with some sand. The high resistivity around 8000 $\Omega.m$ implies a very dry medium.
- Layer 3: No more information is known from the drillings, but the low resistivity (around 7$\Omega.m$) shows that the medium, probably still clay, is wet.

A problem that appears here is that the drop of resistivity appears for both sites around 80 m depth, which seems to indicate that the groundwater table is way below the level that was expected (between 20 and 40 m). Moreover, the results from the MRS appeared to show that the groundwater table from the hydrogeological map of Benin (Lucien et al. 2012, Figure 10) was correct.
This might be caused by the highly resistive layer measured near the surface that may mask the transition between the dry and wet medium by encompassing all of it in a big layer.

3.1.3 Comparison with the results on the Allada plateau

For the top of the aquifer, the MRS gives results that seem coherent with the isopiezometric lines from the hydrogeological map of Benin (Lucien et al. 2012, Figure 10): the top of the aquifer is detected around 37 m deep, and the measurements were made near the 40 m isopiezometric line. These results also appear coherent with the results on the Allada plateau, with the top of the aquifer situated between 60 m in the north and almost 0 m in the south (as shown on the Figure 30), which was expected based on the isopiezometric lines from the hydrogeological map of Benin.

However, the clayey substratum that is identified in Figure 10 between -50 and -120 m AMSL doesn't appear on the MRS, the clay layer might be too deep.

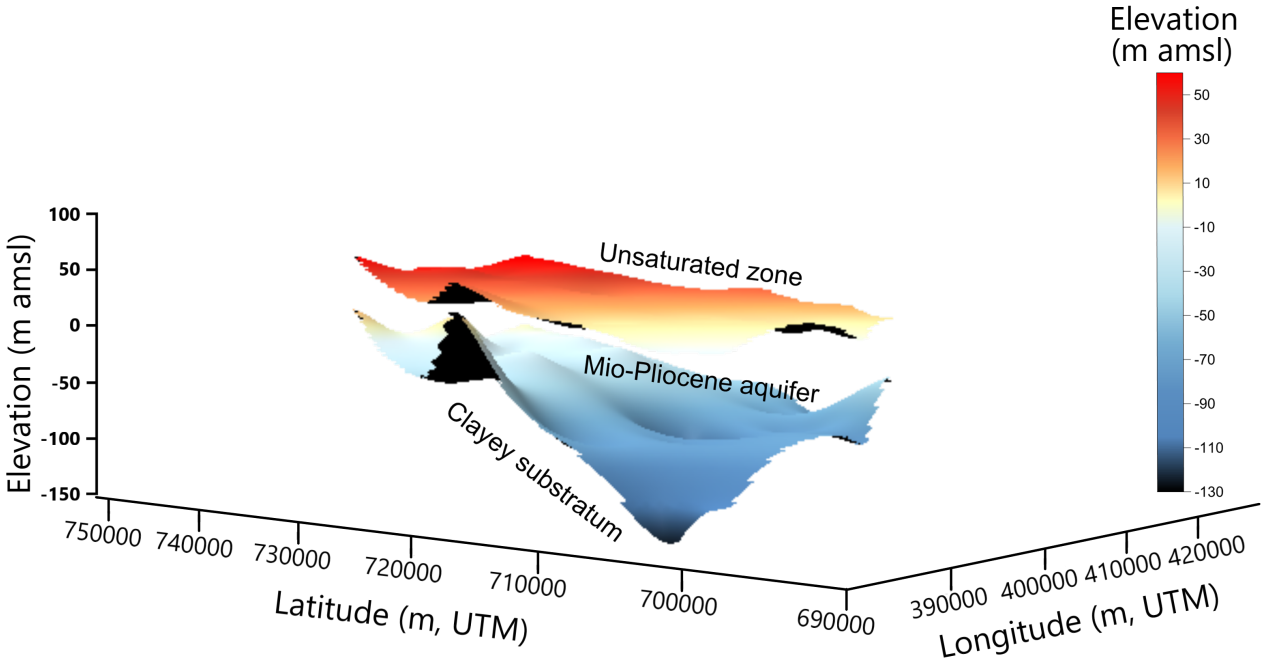

Figure 30: Geometry of the Mio-Pliocene aquifer on the Allada plateau, taken from the presentation of the firsts results of the ongoing study of the plateau, thickness varying between 45 m in the north and 85 m in the south. The top (red to yellow) layer represents the top of the aquifer, and the bottom (blue) layer represents the bottom of the aquifer.

The TDEM gives information on the resistivity of the different layers. The Table 5 shows the resistivity model and associated lithologies for the site of SEKOU in the Allada plateau. By comparing this result with the two models from the Sakété plateau (sites MAIRIE, Table 3 and EPP BAODJO, Table 4), it appears that the results of the site MAIRIE are quite similar, with also 4 layers and the same range of resistivity values (a first layer in the order of 100 $\Omega.m$ that is linked to the unsaturated soil, the second layer with a high resistivity in the order of 1000 $\Omega.m$ of clay, and then the last two layers with decreasing resistivity of sand and clayey sand).
The results for the site EPP BAODJO are a bit different, but there is still a low resistivity layer, then a high resistivity and the last layer has once again a low resistivity.

Layer	Resistivity $[\Omega.m]$	Thickness $[m]$	Depth $[m]$	Lithology
1	68.3	6	6	Laterite
2	2000	50	56	Clay
3	200	60	116	Sand, clayey sand
4	3	24	140	

Table 5: Summary of the resistivity model and lithology obtained from a drilling for the site SEKOU, representative of the Allada plateau

3.2 Chemistry and isotopes

To further characterize the Sakété plateau, some water samples were taken from the different reference piezometers on the Sakété plateau and from a gushing water well at the border of the

plateau, the point Hétin-Sota. The Figure 31 shows the locations that were sampled.
By analysing the ionic and isotopic compositions of the water present on the plateau, it will be possible to know its origin and to see if there are some differences in water composition between the Allada and Sakété plateaus.

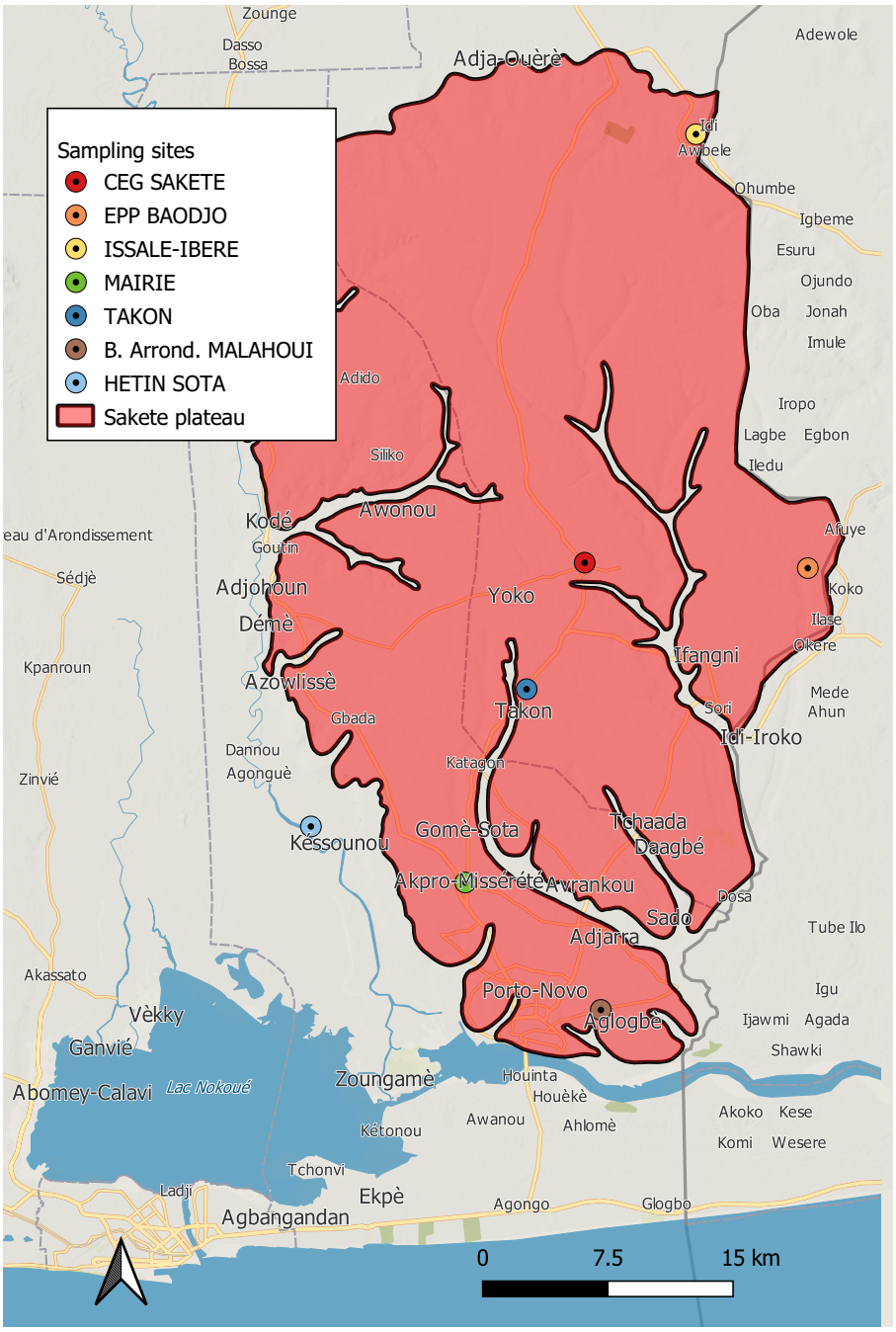

Figure 31: Location of the sites where the sampling was carried out

3.2.1 Acquisition of the data

The water samples were obtained during the internship with the DGeau and the INE. To do so, a pump was used to extract water from the different boreholes. For each borehole, the changes

in electrical conductivity and pH were tracked. When a plateau was observed, the sampling was done inside two plastic bottles (one as is and one acidified) for the ions and inside a glass bottle for the isotopes. The procedure for each water sampling can be found in the Appendix A.3.
For the site Hétin-Sota, no pump was needed as it is an artesian well, coming from a deeper aquifer: the Lower Palaeocene aquifer.

The samples were then brought back to Belgium where the major ions were analysed by the Laboratoire d'analyse en phase aqueuse - Hydrogéologie et Géologie de l'Environnement, UEE-ULiège. The isotopic composition analysis was conducted by the laboratory of the Helmholtz Centre for Environmental Research - UFZ, Department Catchment Hydrology, in Germany. The results of the analysis from both laboratories of the different samples are presented in the Table 20 in the Appendix A.4.

3.2.2 Quality of the data

To check the quality of the data, the ionic balance was first computed using the following formula:

$$\frac{\sum \text{cation} - \sum \text{anion}}{\sum \text{cation} + \sum \text{anion}} \cdot 100(\%)$$

The total cations and anions (in meq/L) were also compared to the electrical conductivity corrected to 25 °C (EC_{25}, in μS/cm) divided by 100. These three values should be of the same order to check the validity of the data.
The Table 6 shows the values of these quality markers. It can be seen that the ionic balance is lower than 5 % for all sites except for ISSALE IBERE where it is at 6.99 %. An ionic balance lower than 5 % is considered correct in terms of electro neutrality (Deutsch and Siegel 1997), the higher value for ISSALE IBERE might indicate that there is a slight error with this data, but still within acceptable range.
The "maximum error" on the last column is the maximum error between the total anion or cation and the electrical conductivity divided by 100, in % computed by the equation:

$$MAX\left(\frac{|Conductivity/100 - Total\ cations|}{Conductivity/100}, \frac{|Conductivity/100 - Total\ anions|}{Conductivity/100}\right) * 100 \quad (1)$$

	Ionic balance [%]	Total cations [meq/L]	Total anions [meq/L]	$EC_{25}/100$ [μS/cm]	Error max [%]
CEG SAKETE	-3.69	0.47	0.51	0.53	10.587
ISSALE IBERE	-6.99	1.09	1.25	0.93	34.697
EPP BADUDJO	-4.62	0.43	0.47	0.49	12.565
TAKON	-3.24	0.79	0.84	0.86	8.153
AKPRO MISSERETE	-4.73	0.74	0.81	0.94	21.320
MALAHOUI	-4.16	0.35	0.38	0.45	21.133
HETIN-SOTA	-1.73	9.54	9.87	9.53	3.601

Table 6: Values of the ionic balance, total cations and anions, conductivity/100 and maximum error between the total anion/cation and the conductivity/100 for the 7 water samples

Once again, the site ISSALE IBERE has the biggest value, with an error of 34.7%, while the rest of the sites have errors lower or around 20%. The data set can thus be considered of good quality overall. It can be noted that the observed concentrations are relatively small, which might induce a higher ionic balance and maximum error with the small denominator.

3.2.3 Analysis of the hydrochemistry

A first observation that can be made is that the sample "HETIN-SOTA" has values that are completely different from the other ones. This is easily explainable because it was taken from an artesian well in the Ouémé valley, whereas the other samples were taken from non-artesian wells from the Sakété plateau.
Comparing the data with those from Kpegli 2020, it appears that two samples have the same range of values : one from the same site (Hétin-Sota) and another one up north (Atchabita), that are from the Palaeocene aquifer. This aquifer is located in limestones and at a high depth, which explains the high temperature and pH. The higher conductivity can be linked to a higher ion concentration (mainly HCO_3^-, K^+, Na^+, Cl^-), however the measured concentrations are still under the World Health Organization (WHO) standards (Organization 2017).
It is interesting to note that the high temperature of the water from Hétin-Sota (measured on site at about 50°C) can induce hazard, as it can enhance the growth of microorganisms.

3.2.3.1 Statistical analysis of the data

To further analyse the data, the minimum, mean, standard deviation and maximum values of the samples (the sample from Hétin-Sota excluded) were computed for the pH, electrical conductivity and ion concentrations in the Table 7. The WHO regulations for the different parameters were also put in the table to see if some values were above the threshold values. The pH is the only value that is below the recommended limits, with values that range from 4.71 to 5.72, which indicates acidic waters. In terms of potability, the water samples are thus all within WHO standards (the WHO doesn't impose a health-based guideline value for pH, as it usually has no direct impact on consumers).

	Minimum	Maximum	Mean	Standard deviation	WHO regulation
Conductivity [μS/cm]	44.8	94.1	69.88	23.44	500
pH	**4.71**	**5.72**	**5.16**	0.44	6.5-8.5
Ca [mg/L]	0.08	0.55	0.26	0.18	300
CO_3^{2-} [mg/L]	0	0	0	0	300
HCO_3^- [mg/L]	0.04	0.46	0.21	0.18	500
Fe [mg/L]	0	0	0	0	2
Mn [mg/L]	0	0	0	0	0.4
K^+ [mg/L]	0.01	0.03	0.01	0.01	/
Li^+ [mg/L]	0	0	0	0	/
Mg^{2+} [mg/L]	0.06	0.12	0.1	0.02	200
Na^+ [mg/L]	0.15	0.4	0.28	0.1	200
NH_4^+ [mg/L]	0	0	0	0	0.2
Sr^{2+} [mg/L]	0	0.01	0	0	7
Br^- [mg/L]	0	0	0	0	2
Cl^- [mg/L]	0.22	0.34	0.28	0.04	250
F^- [mg/L]	0	0.01	0	0	1.5
NO_3^- [mg/L]	0	0.44	0.11	0.17	50
PO_4^{3-} [mg/L]	0	0.38	0.06	0.16	1
SO_4^{2-} [mg/L]	0	0.09	0.04	0.04	250

Table 7: Statistical analysis of the electrical conductivity, pH and main ion concentrations for the 6 sites on the Sakété plateau and WHO regulations

3.2.3.2 Graphical representation of the dataset

The data were then plotted as Piper (Figure 32), Stiff (Figure 39, in the Appendix A.5), Stabler (Figure 40, in the Appendix A.5) and Schöeller-Berkaloff (Figure 41, in the Appendix A.5) diagrams using the software Diagrammes.
The Piper diagram (Table 32) shows once again that the water from Hétin-Sota is different from the rest, being a sodium, potassium and chloride bicarbonate water, while the rest of the samples are of similar composition : chlorinated and sulphated calcium and magnesium water without dominant cations.
The Stiff (Figure 39), Stabler (Figure 40) and Schöeller-Berkaloff (Figure 41) diagrams show that the waters aren't exactly the same, with different profiles with varying contents of ions, but still in the same range of concentration.

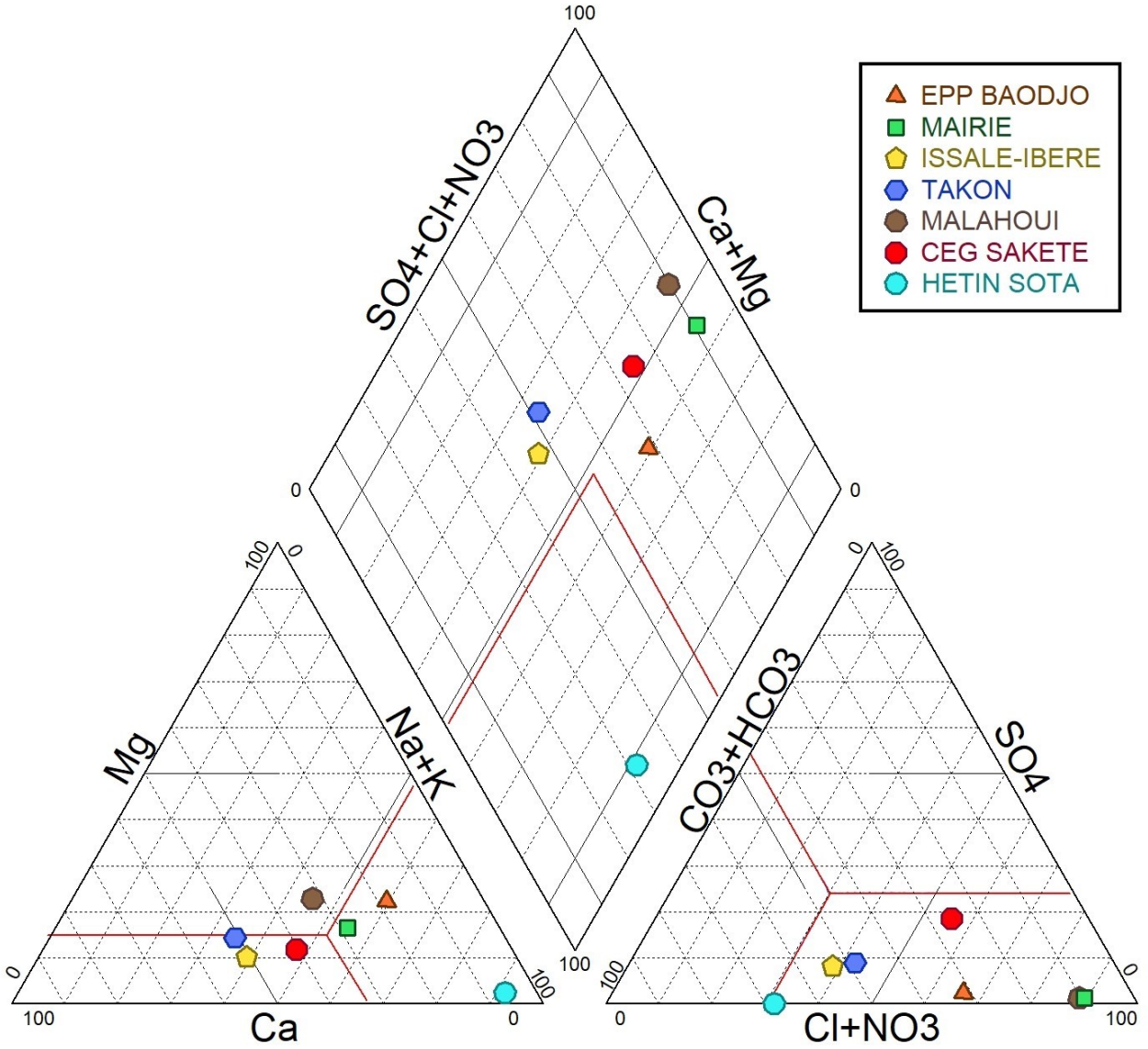

Figure 32: Piper diagram of the water samples

3.2.4 Analysis of the isotopic composition of the water samples

The water samples were analysed for their isotopic fractions for two isotopes: deuterium (δ^2H) and oxygen-18 (δ^{18}O). The results are available at the end of the Table 20 in the Appendix A.4.

The isotopic content of the water samples in δ^2H and δ^{18}O, in ‰, is plotted in Figure 33. To compare these results, the Global Meteoric Water Line ($\delta^2\text{H} = 8\delta^{18}\text{O} + 10$) and the Local Meteoric Water Line ($\delta^2\text{H} = 7.5\delta^{18}\text{O} + 10$, according to Odeloui et al. 2022, based on long-term monthly rainwater data obtained from the station of Abomey-Calavii) were also plotted, as well as the rainfall weighted mean.

Looking at the plotted isotopic contents, it can be seen that the water samples are close to the mean rainfall isotopic content, and quite close to the Local Meteoric Water Line. The water

from the Mio-Pliocene aquifer is thus relatively recent and comes mainly from rainfall, contrary to the water from Hétin-Sota (Lower Palaeocene aquifer), which is strongly depleted in both δ^2H and δ^{18}O and is thus a paleo-groundwater, coming from a more ancient rainfall.

The Ouémé river (from Kpegli 2020, sample taken near Dangbo) and seawater (from Odeloui et al. 2022) isotopic content were also plotted to compare the data. The Ouémé river does not appear to influence the water, but the isotopic content of the Ouémé river is in between both aquifers, which can suggest that the Ouémé river is the result of the mix between water from both the Mio-Pliocene and Lower Palaeocene aquifers.

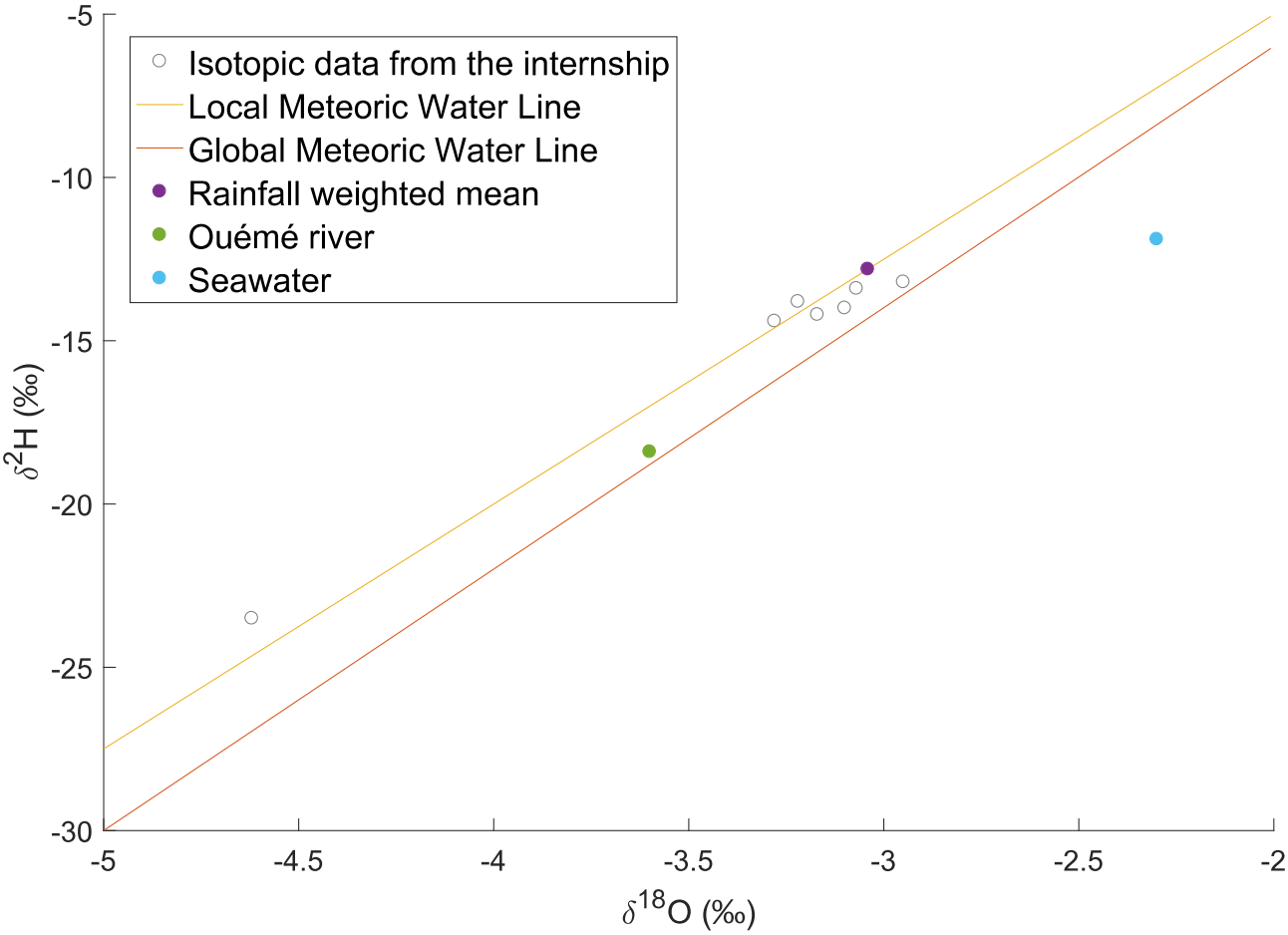

Figure 33: Isotopic content of the water samples, plus the Local Meteoric Water Line, Global Meteoric Water Line, rainfall weighted mean, Ouémé river and seawater isotopic content

3.2.5 Comparison with the data from the Allada plateau

In the paper "Chemical evolution of the continental terminal shallow aquifer in the south of coastal sedimentary basin of Benin (west-Africa) using multivariate factor analysis", Abdoukarim Alassane et al. 2015, the data from both the Allada and Sakété plateaus are treated as one, as the sampled aquifer is from the same geological formation (Mio-Pliocene, or Continental Terminal in the paper).
However, the majority of the samples taken near Porto-Novo and its lagoon have a high electrical conductivity, which can be linked to the intrusion of seawater and a high salt concentration,

thus the computed mean values encompass two type of water : the fresh water from the aquifer and the mix between the fresh water and seawater. To avoid comparing the salty waters and the waters from the plateaus, an arbitrary limit on the electrical conductivity was fixed to the mean value of the dataset : 201 μS/cm. Over 76 % of the samples are still included in this selection, from which only the samples taken from boreholes or wells on the plateaus are taken. This gives 45 samples, 18 on Sakété and 27 on the Allada plateau. Adding the 6 samples taken on Sakété during the internship gives 24 samples on Sakété. The quality of the data taken from Alassane et al. is good, with all ionic balances lower than 5 % for the samples.

The following Piper diagram (Figure 34) shows the composition of the 51 water samples. The data from Alassane et al. seem to show a clear difference between both plateaus : the water samples from the Allada plateau are chloride and sulphate or Bi/carbonate, calcium and magnesium waters, while the water samples from the Sakété plateau are chloride sodium/sulphate and potassium waters. This suggests a difference between both aquifers, thus the choice to treat the whole dataset as one can be questioned. Furthermore, looking at the repartition of the electrical conductivities on the plateau, the location near the Porto-Novo lagoon has really high values due to the mix with seawater and could thus be treated as another group, further questioning the choice to treat the whole dataset as one.

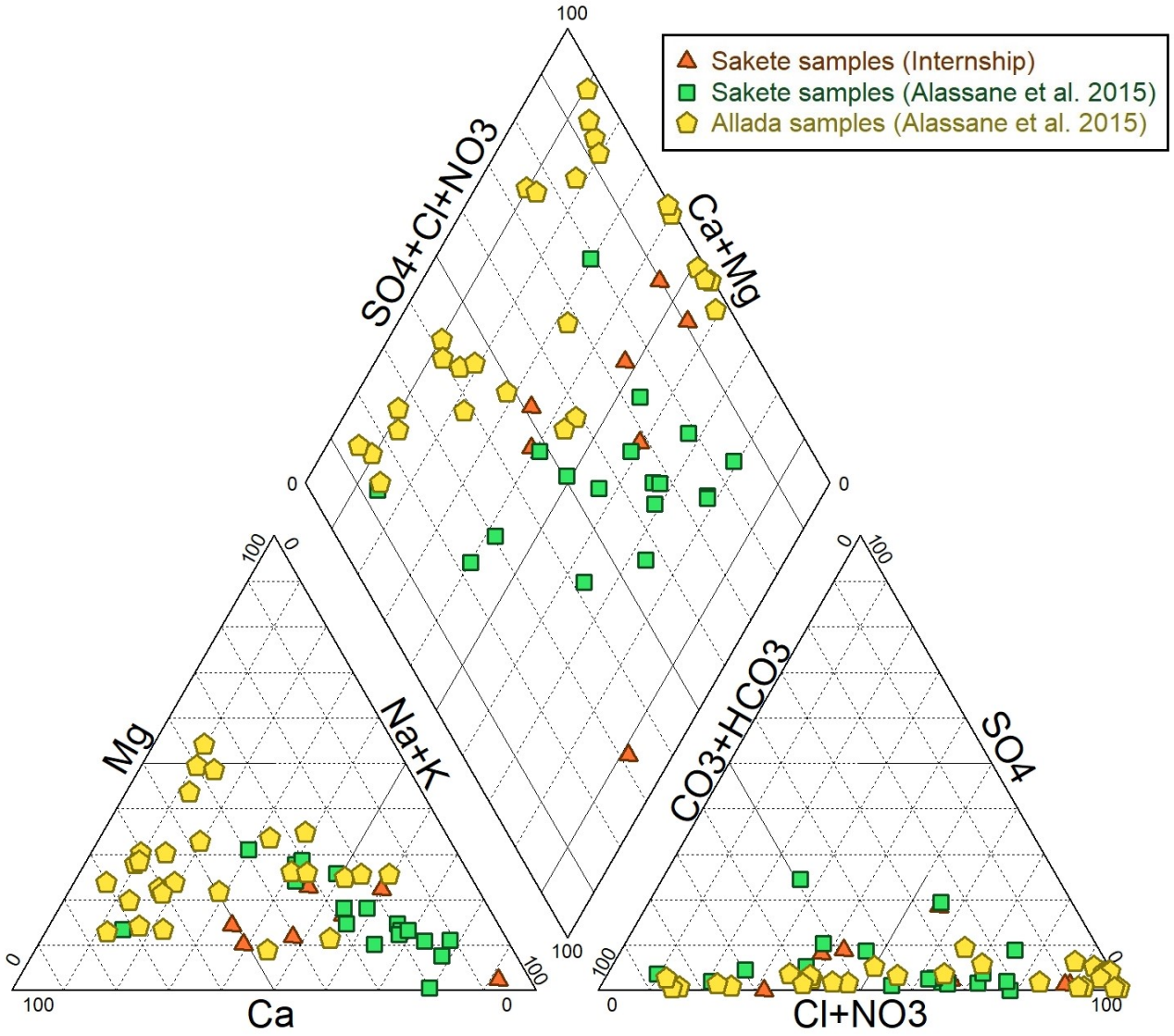

Figure 34: Piper diagram of the water samples for Allada and Sakété

The data collected during the internship on the Sakété plateau are in the middle of the waters from both plateaus, with the average values of the samples from the internship close to the average values from Abdoukarim Alassane et al. 2015. However, it is complicated to compare the results from Abdoukarim Alassane et al. 2015 and the ones obtained during the internship, as they weren't analysed by the same laboratories, and they were taken 6 years apart.

However, it can be noted that the main difference between the Sakété and Allada samples lies in the cations. By taking a closer look at the cation triangle, the data from Sakété appear to be aligned. This can be linked to two phenomenons, either there is a mix with deeper waters, or there is an ion exchange (Ca/Na) with a clay layer. The former seems to be more probable as the alignment of the cations seems to coincide with the water sample from Hétin-Sota, which is from a deeper aquifer (lower Paleocene aquifer).

An attempt was made to try to see if there was a correlation between the data from Alassane et al. and the data from the internship. However, only two points were identified to be close: Sakété and the point 15, and Takon and the point number 7, and they have a totally different

ionic signature, with only the NA+K pole at a similar percentage (about 90%) on the Piper diagram.

3.3 NASA POWER data

The Prediction of Worldwide Energy Resources (POWER) Project is a NASA program that allows free access to environmental data (solar and meteorological data from NASA research) worldwide for support of renewable energy, building energy efficiency and agricultural needs (according to the POWER website, NASA 2022). These data are satellite-based data, and come from two different sources :

- The meteorological data are based on NASA's Modern Era Retrospective-Analysis for Research and Applications (MERRA-2) model from the Goddard's Global Modeling and Assimilation Office (GMAO) (Gelaro et al. 2017);
- The solar data are based on the analysis of satellite imagery done by NASA's Global Energy and Water Exchange Project (GEWEX) and NASA's Clouds and the Earth's Radiant Energy System (CERES).

The NASA POWER data were downloaded from the online POWER Data Access Viewer. A point was selected for each plateau, near the cities of Allada and Sakété. Both locations are in the centre of the plateaus and around the same distance from the coast to be representative of the entirety of the plateaus. They are represented on Figure 35
For each point, 6 parameters were selected to compute the reference evapotranspiration (ET_0) using the software ET0 Calculator :

- ALLSKY_SFC_SW_DWN : CERES SYN1deg All Sky Surface Shortwave Downward Irradiance (kW-hr/m^2/day)
- WS2M : CMERRA-2 Wind Speed at 2 Meters (m/s)
- T2M_MAX : CMERRA-2 Temperature at 2 Meters Maximum (C)
- T2M_MIN : CMERRA-2 Temperature at 2 Meters Minimum (C)
- RH2M : CMERRA-2 Relative Humidity at 2 Meters (%)
- PRECTOTCORR : CMERRA-2 Precipitation Corrected (mm/day)

The data were downloaded daily for the period 01/01/1990 through 12/31/2021, for a total of 11 688 data set for each point.

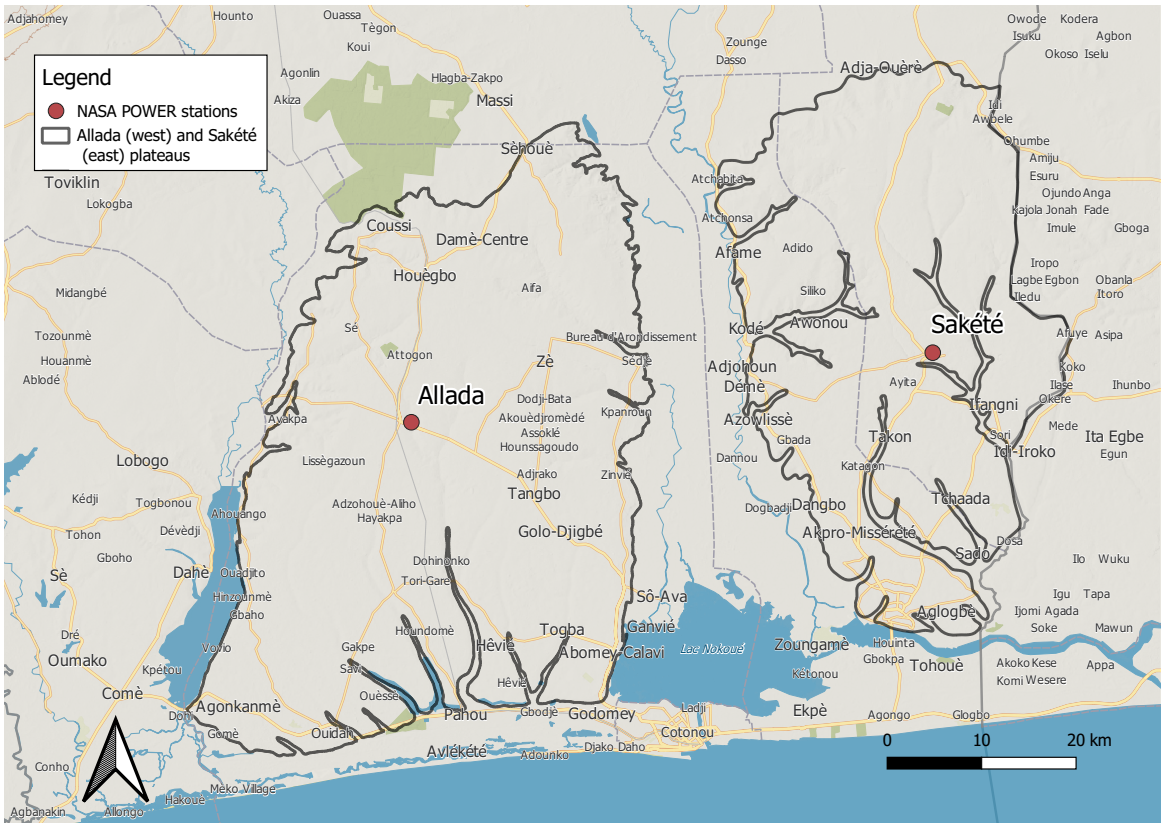

Figure 35: Position of the two selected points for the NASA POWER data on the Allada and Sakété plateaus

3.3.1 Analysis of the data

The ET_0 was computed using the software ET0 Calculator, which uses the FAO Penman-Monteith equation (Allen et al. 1998):

$$ET_0 = \frac{0.408\Delta\,(R_n - G) + \gamma \frac{900}{T+273} u_2\,(e_s - e_a)}{\Delta + \gamma\,(1 + 0.34u_2)} \tag{2}$$

where
- ET_0 reference evapotranspiration $[\text{mm day}^{-1}]$,
- R_n net radiation at the crop surface $[\text{MJ m}^{-2}\text{ day}^{-1}]$,
- G soil heat flux density $[\text{MJ m}^{-2}\text{ day}^{-1}]$,
- T mean daily air temperature at 2 m height $[°C]$,
- u_2 wind speed at 2 m height $[\text{m s}^{-1}]$,
- e_s saturation vapour pressure [kPa],
- e_a actual vapour pressure [kPa],
- $e_s - e_a$ saturation vapour pressure deficit [kPa],
- Δ slope vapour pressure curve $[\text{kPa }°\text{C}^{-1}]$
- γ psychrometric constant $[\text{kPa }°\text{C}^{-1}]$

Using the computed ET_0 and the daily precipitation, it was possible to compute the ET_R and the effective water using the Thornthwaite method (with a maximum storage set to the commonly used value of 100 mm) over the span of over 30 years, from 1990 to 2021.
The figures 36 and 37 show the annual sum of the studied parameters : precipitations, ET_0, ET_R

and effective water, respectively in Sakété and Allada. It appears that the yearly precipitations and effective water in Allada are lower than in Sakété, which is coherent with the difference in precipitation observed in Figure 3. The mean annual values for Allada are : 1 143 mm/year of precipitation and 189.07 mm/year of effective water, while the values for Sakété are 1 288.6 mm/year of precipitation and 316.57 mm/year of effective water.

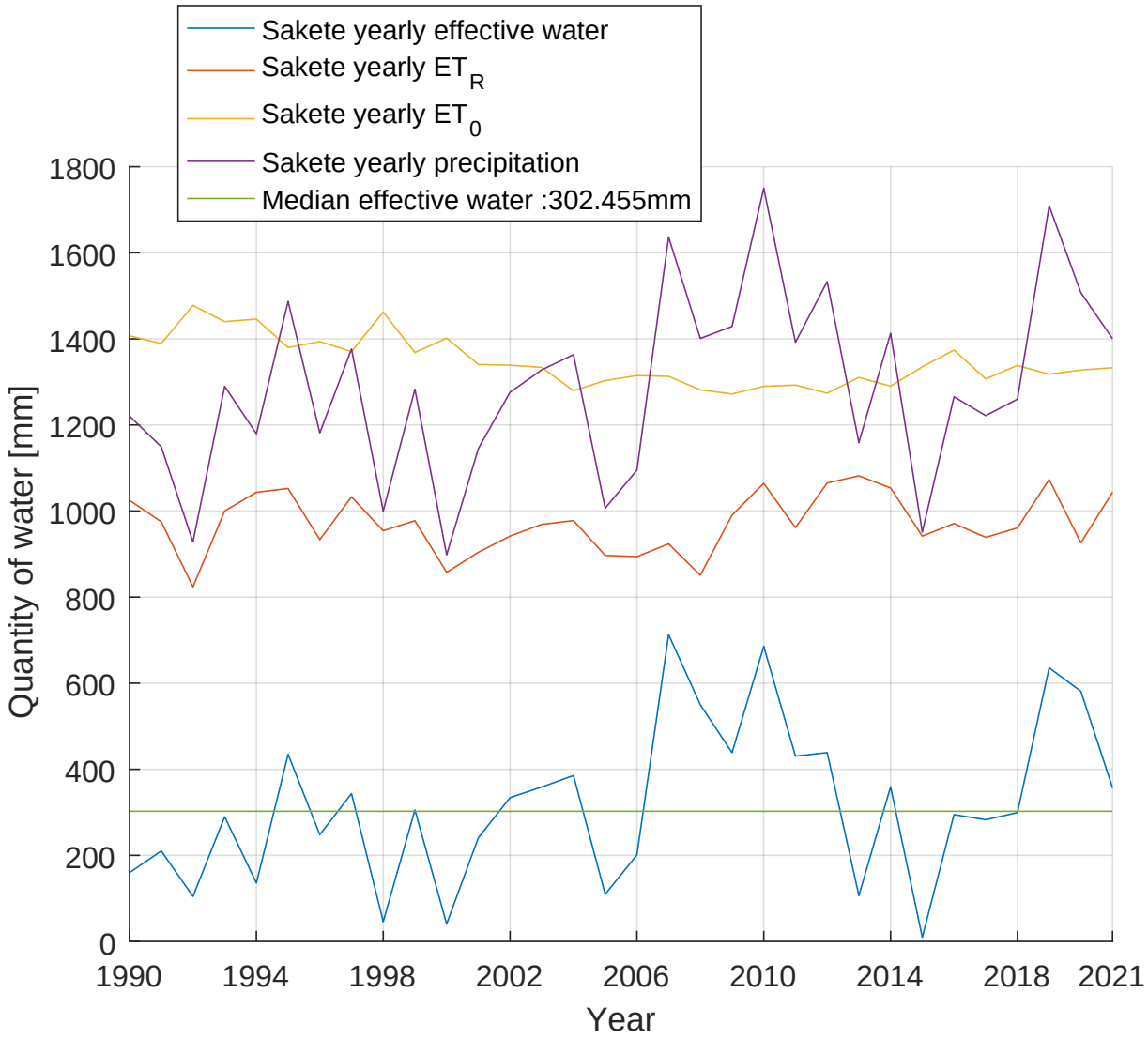

Figure 36: Annual sum of the precipitations, ET_0, ET_R and effective water from 1990 to 2021 in Sakété

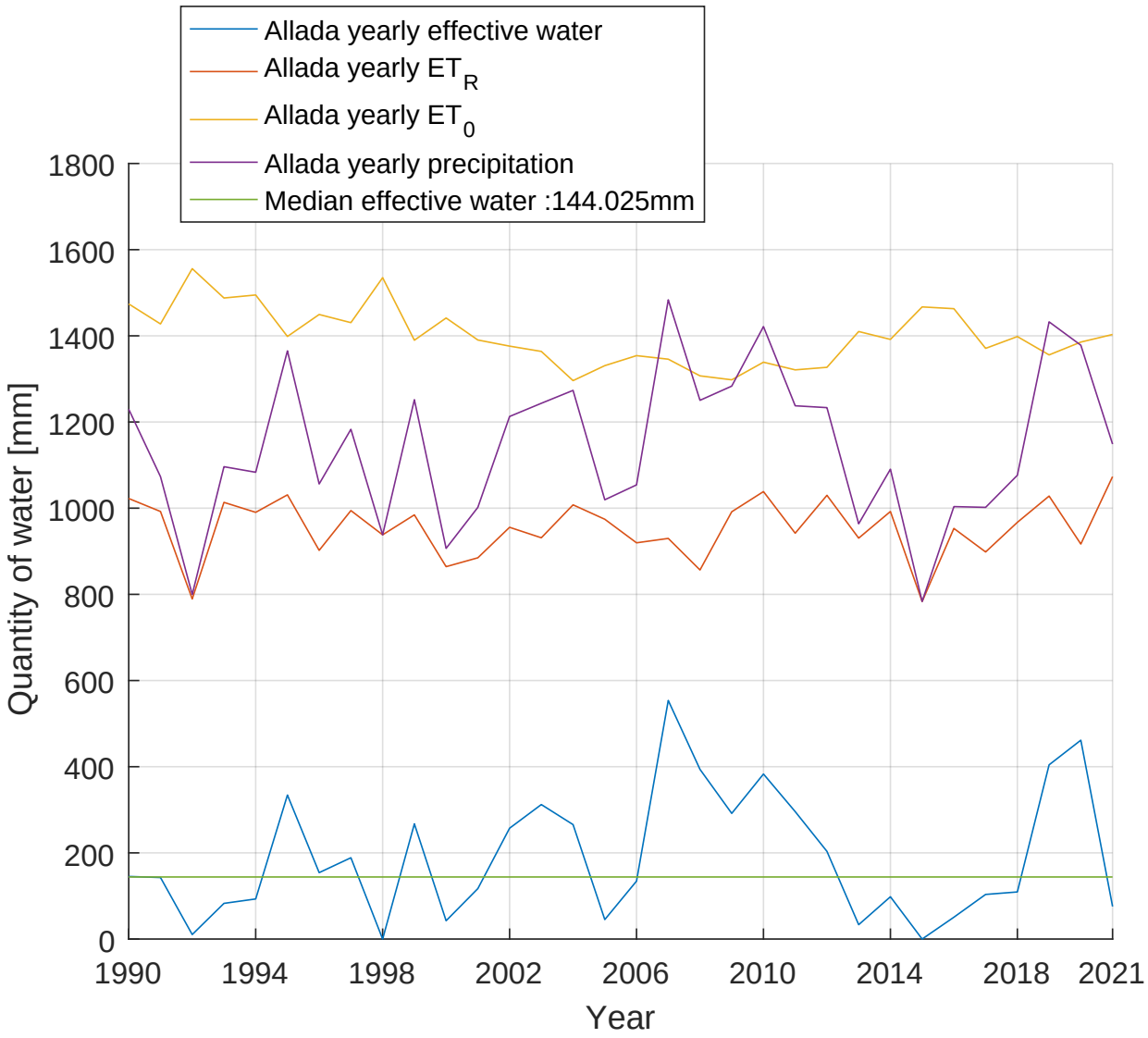

Figure 37: Annual sum of the precipitations, ET_0, ET_R and effective water from 1990 to 2021 in Allada

4 Conclusion

This thesis aimed to conduct a preliminary hydrogeological characterization of the Sakété plateau in the coastal sedimentary basin of Benin, and more precisely of the Mio-Pliocène aquifer.

First, using the geophysical surveys of both Time-domain electromagnetic (TDEM) and Magnetic Resonance Sounding (MRS), it was possible to compare the hydrogeological context of the studied plateau and the plateau of Allada. The interpretation of the data obtained by both methods showed that both plateaus are quite similar in terms of geology and piezometric levels :

The TDEM showed results that were similar in the studied sites on the Sakété plateau and on the site of SEKOU, representative of the Allada plateau. Indeed, the same succession of resistivity layers can be observed in both cases: a first layer in the order of 100 $\Omega.m$ that is linked to the unsaturated soil, the second layer with a high resistivity in the order of 1000 $\Omega.m$ of clay, and then the last two layers with decreasing resistivity of sand and clayey sand.

The MRS showed a piezometric level for the point of measurement that is coherent with the isopiezometric lines from the hydrogeological map of Benin (Lucien et al. 2012), with the top of the aquifer being detected around 37 m deep, while the measurements were made near the 40 m isopiezometric line according to the hydrogeological map of Benin.
The geometry of the aquifer of the Allada plateau (Figure 30), shows that the top of the aquifer is situated between 60 m in the north and almost 0 m in the south, which is also in accordance with the isopiezometric lines from the hydrogeological map of Benin.
This shows that the isopiezometric lines as drawn in the hydrogeological map of Benin are correct (at least for the point of measurement), and comparing both plateaus based on these lines, they appear really similar.
The analysis of water samples taken in locations distributed on the Sakété plateau gave two information through the isotopic and ionic contents of the water:

In terms of isotopic content, the water samples from the plateau showed waters with an isotopic content close to the precipitations, indicating that the waters are recent, in opposition to the water from the aquifer situated below (lower Paleocene aquifer), taken in the site of Hétin-Sota, which is strongly depleted in both δ^2H and δ^{18}O and is thus a paleo-groundwater, coming from more ancient rainfalls. An interesting observation is that the isotopic signature of the Ouémé river seems to indicate that it is composed of a mix between the water of both aquifers, meaning that the Ouémé river is draining.

The ionic analysis showed low ionic concentrations for the samples taken during the study, with values within the World Health Organization standards. The water samples from the plateau were all chlorinated and sulphated calcium and magnesium waters without dominant cations (while the water from the lower Paleocene aquifer was a sodium, potassium and chloride bicarbonate water). Comparing these results with the data from Abdoukarim Alassane et al. 2015, the graphical representation of a Piper diagram showed a difference in cation composition between the water from the plateaus. The waters from the Sakété plateau show the signature of an ion exchange (due to the presence of clay) or a mix with the deeper water from the lower Paleocene aquifer. If the second hypothesis is the correct one, then there might be an additional water intake coming from the aquifer underneath.

Regarding the precipitations and recharge, it can be seen that the Sakété plateau is subjected to about 13% more precipitations than the Allada plateau. This added percentage in precipitation, once computed using the software ET0 Calculator with other parameters (downward irradiance, wind speed, temperature and humidity) and using the Thornthwaite method, gives 67% more effective water for the Sakété plateau than on the Allada plateau.

Compiling all of these information, it can be said that both plateaus have a similar geology, but both systems appear a bit different, with different ionic concentrations. However, in terms

of water contents and recharge, for a first estimation, taking the same values as the Allada plateau (rescaled to fit the size of the Sakété plateau) appear to be a conservative assumption, taking into account that the Sakété plateau has more effective water and a possible water intake coming from the aquifer underneath.
Of course, a more detailed study, with more samples and geophysical measurements still needs to be conducted to confirm the conclusion of this thesis, as only few measurements were made due to a lack of time.

References

[1] ABEM. *ABEM WalkTEM Users Guide*. 2016. URL: https://americasguidelin.cdn.triggerfish.cloud/uploads/2016/03/ABEM-WalkTEM-Users-Guide-33-8000-97-20140930.pdf.

[2] J.-B. Achidi, L. Bourguet, R. Elsaesser, A. Legier, E. Paulvé, and N. Tribouillard. *Carte Hydrogéologique du Bénin, Carte de l'ensemble du territoire à l'échelle 1/500.000 - Notice Explicative*. Ed. by Deutsche Gesellschaft für Internationale Zusammenarbeit (GIZ) GmbH. Jan. 2012.

[3] J.-B. Achidi, L. Bourguet, R. Elsaesser, A. Legier, E. Paulvé, and N. Tribouillard. *Carte Hydrogéologique du Bénin, Carte du Bassin Sédimentaire Côtier à l'échelle 1/200.000 - Notice Explicative*. Ed. by Deutsche Gesellschaft für Internationale Zusammenarbeit (GIZ) GmbH. Jan. 2012.

[4] National Aeronautics and Space Administration (NASA). *About the Prediction Of Worldwide Energy Resources (POWER) Project*. 2022. URL: https://www.arcgis.com/home/item.html?id=52116d331ff64e468fe9351fc1c76423 (visited on 05/12/2022).

[5] A. Alassane. "Étude hydrogéologique du Continental Terminal et des formations de la plaine littorale dans la région de Porto-Novo (Sud du Bénin) : identification des aquifères et vulnérabilité de la nappe superficielle". PhD thesis. Univ. C. A. Diop of Dakar, 2004.

[6] Abdoukarim Alassane, Rim Trabelsi, Léonce F Dovonon, Diane J Odeloui, Moussa Boukari, Kamel Zouari, and Daouda Mama. "Chemical evolution of the continental terminal shallow aquifer in the south of coastal sedimentary basin of Benin (west-Africa) using multivariate factor analysis". In: *J. Water Resource Prot.* 07.06 (2015), pp. 496–515.

[7] Richard Allen, Luis Pereira, Dirk Raes, and Martin Smith. *Crop evapotranspiration - Guidelines for computing crop water requirements*. Rome, Italy: FAO Irrigation and Drainage Paper N° 56, 1998. ISBN: 92-5-104219-5.

[8] E. C. Alohou, D. S. J. C. Gbemavo, Sylvanus Mensah, and C. Ouinsavi. "Fragmentation of Forest Ecosystems and Connectivity Between Sacred Groves and Forest Reserves in Southeastern Benin, West Africa". en. In: *Tropical Conservation Science* 10 (Jan. 2017), p. 1940082917731730. ISSN: 1940-0829. DOI: 10.1177/1940082917731730.

[9] E. Amoussou, S.H. Totinvodounon, F.P. Cledjo, Y.B.S. Allagbe, J.S.A. Akognongbe, C. Houndenou, G. Mahe, P. Camberlin, M. Boko, and J.Perard. "Évolution climatique du Bénin de 1950 a 2010 et son influence sur les eaux de surface". In: *XXIXe Colloque de l'Association Internationale de Climatologie: « Climat et pollution de l'air »*. Besançon, France, 2016.

[10] Deborah Balk, Tom Pullum, Adam Storeygard, Fern Greenwell, and Melissa Neuman. *Spatial analysis of childhood mortality in West Africa*. 2003. URL: http://dhsprogram.com/pubs/pdf/SAR5/SAR5.pdf.

[11] Fêmi Cocker, Jean Bosco Vodounou, and J. Yabi. "Évolution récente des débits dans la basse vallée de l'Ouémé, Sud-Benin". In: *Journa de Physique de la SOAPHYS* 1 (Dec. 2019), C19A1–1. DOI: 10.46411/jpsoaphys.19.01.001.

[12] Jeffrey J. Danielson and Dean B. Gesch. *Global Multi-Resolution Terrain Elevation Data 2010 (GMTED2010)*. Ed. by U.S. Geological Survey (USGS) Earth Resources Observation and Science (EROS). 2011. URL: https://earthexplorer.usgs.gov/scene/metadata/fgdc/5e83a1f36d8572da/GMTED2010S10E000/.

[13] William J Deutsch and Randy Siegel. *Groundwater Geochemistry: Fundamentals and Applications to Contamination*. CRC Press, 1997.

[14] Food and Agriculture Organization of the United Nations. *World reference base for soil resources 2006: A framework for international class*. Rome, Italy: Food & Agriculture Organization of the United Nations (FAO), 2006.

[15] Ronald Gelaro, Will McCarty, Max J. Suárez, Ricardo Todling, Andrea Molod, Lawrence Takacs, Cynthia A. Randles, Anton Darmenov, Michael G. Bosilovich, Rolf Reichle, Krzysztof Wargan, Lawrence Coy, Richard Cullather, Clara Draper, Santha Akella, Virginie Buchard, Austin Conaty, Arlindo M. da Silva, Wei Gu, Gi-Kong Kim, Randal Koster, Robert Lucchesi, Dagmar Merkova, Jon Eric Nielsen, Gary Partyka, Steven Pawson, William Putman, Michele Rienecker, Siegfried D. Schubert, Meta Sienkiewicz, and Bin Zhao. "The Modern-Era Retrospective Analysis for Research and Applications, Version 2 (MERRA-2)". In: *Journal of Climate* 30.14 (July 2017), pp. 5419–5454. DOI: 10.1175/jcli-d-16-0758.1. URL: https://doi.org/10.1175/jcli-d-16-0758.1.

[16] Aarhus GeoSoftware. *SPIA-TEM Manual*. 2022. URL: http://www.ags-cloud.dk/Wiki/S_SPIATEMManual.

[17] The World Bank Group. *Benin - Climatology | Climate Change Knowledge Portal*. 2021. URL: https://climateknowledgeportal.worldbank.org/country/benin/climate-data-historical (visited on 05/13/2022).

[18] IGRAC. *Les Eaux Souterraines face à l'Explosion Urbaine en Afrique de l'Ouest (map)*. 2021.

[19] Philip Kearey, Michael Brooks, and Ian Hill. *An Introduction to Geophysical Exploration*. en. 3rd ed. Philadelphia, PA: Blackwell Science, Mar. 2002.

[20] N. S. Kindohoundé, L. Nodichao, N. S. H. Aholoukpè, and A. Saïdou. "Mapping of soil nutrient deficiency in oil palm plantations of Southern Benin". en. In: *African Crop Science Journal* 29.1 (2021), pp. 141–156. ISSN: 2072-6589. DOI: 10.4314/acsj.v29i1.10.

[21] K. a. R. Kpegli. "Flow characterization and modelling of a South Benin artesian aquifer system: Effects of hydraulic and storage properties and recharge on simulated heads across the artesian zone". English. In: (2020). DOI: 10.18174/526095.

[22] Luc Le Barbé, Grégoire Alé, Bertrand Millet, Hervé Texier, Yves Borel, and René Gualde. *Les ressources en eaux superficielles de la République du Bénin*. Monographies Hydrologiques. ORSTOM, 1993, p. 540. ISBN: 2-7099-1168-X. URL: https://www.documentation.ird.fr/hor/fdi:39537.

[23] Bourguet Lucien, Paulve Eric, Legier André, Tribouillard Nicolas, and Achidi Jean-Babtiste. *Carte Hydrogéologique Du Bénin 1/500.000*. Ed. by Deutsche Gesellschaft für Internationale Zusammenarbeit (GIZ) GmbH. Jan. 2012. URL: https://www.pseau.org/outils/ouvrages/giz_dgeau_carte_hydrogeologique_du_benin_2012.pdf.

[24] Ministère de l'Eau et des Mines du Bénin. *Fiche synoptique du programme OMIDELTA*. 2020. URL: https://ressources-eau.gouv.bj/pages/24-programme-omidelta (visited on 05/12/2022).

[25] A. Neven, P. K. Maurya, A. V. Christiansen, and P. Renard. "tTEM20AAR: a benchmark geophysical data set for unconsolidated fluvioglacial sediments". In: *Earth System Science Data* 13.6 (2021), pp. 2743–2752. DOI: 10.5194/essd-13-2743-2021.

[26] Diane Odeloui, Bertil Nlend, Frédéric Huneau, Hélène Celle, Emilie Garel, Abdoukarim Alassane, Moussa Boukari, and Gédéon Sambienou. "Insight into Groundwater Resources along the Coast of Benin (West Africa) through Geochemistry and Isotope Hydrology; Recommendations for Improved Management". In: *Water* 14.14 (2022). DOI: 10.3390/w14142154.

[27] World Health Organization. *Guidelines for drinking-water quality, 4th edition, incorporating the 1st addendum*. 2017.

[28] J. Roy and M. Lubczynski. "The magnetic resonance sounding technique and its use for groundwater investigations". In: *Hydrogeology Journal* 11.4 (Aug. 2003), pp. 455–465. DOI: 10.1007/s10040-003-0254-8. URL: https://doi.org/10.1007/s10040-003-0254-8.

[29] Nestor Sokpon. "Recherches écologiques sur la forêt dense semi-décidue de Pobe au sud-est du Bénin: groupements végétaux, structure, régénération naturelle et chute de litière". PhD thesis. Université libre de Bruxelles, Faculté des sciences, Bruxelles, 1995. URL: http://hdl.handle.net/2013/ULB-DIPOT:oai:dipot.ulb.ac.be:2013/212570.

[30] Pierre-Louis Vincent and Gabriel Hottin. *Carte géologique de la République populaire du Bénin 1/200.000*. Ed. by Ministère de l'Industrie et de l'énergie - Office béninoise des Mines (OBEMINES). Digitalised by Ulrich Weller and Marie-Rufine Agbo (Institute of Soil Science and Land Evaluation University of Hohenheim, Germany). 1984. URL: https://projekte.uni-hohenheim.de/atlas308/c_benin/projects/c2_1_1/html/french/btext_fr_c2_1_1.htm.

A Appendix

A.1 Legend of the Hydrogeological map of Benin

Age	No de la zone	Figuré	Facies, lithologie et caractéristiques des unités	Nombre des forages	Profondeur des forages (m)	Niveau de l'eau (m)	Débit spécifique Qs moyen ($m^3/h/m$)	Débit max. d'essai moyen (m^3/h)	% de réussite	Notes supplémentaires
Quaternaire	1		Dépôts de cordon littoral et lagunaires argile, sable et niveaux charbonneux	12	20 à 100	3	7,0	15,9	100	Risque élevé d'intrusion saline; les forages les moins profonds (< 30 m) captent les sables Quaternaire
	2		Alluvions dans la zone de socle galets, graviers, sable, terre sableuse	2	-	-	-	-	-	
	2a		Alluvions récentes des vallées du Bassin Sédimentaire Côtier (BSC) sable, argile, graviers et niveaux charbonneux	3	-	-	-	-	-	
	2b		Alluvions récentes et terrasses anciennes des dépressions de l'Ouémé, du Mono et du Couffo; sable, argile, graviers et niveaux charbonneux	159	20 à 400	7	7,3	11,6	87	En cas d'échec dans les alluvions du Quaternaire, les forages récents récents sont descendus dans les trois aquifères sous-jacents : Mio-Pliocène, calcaires de l'Eo-Paléocène ou sables du Crétacé
	3		Alluvions récentes du Niger sable fin	14	20 à 50	8	1,1	4,8	100	
	4		Alluvions récentes de la Pendjari sable	0	-	-	-	-	-	
	5a		Biseau sec des plateaux Mio-Pliocène BSC	37	50 à 450	37	1,5	7,5	54	Secteur difficile : le Mio-Pliocène est stérile. Les forages positifs dans les calcaires Eo-Paléocène ou sables du Crétacé sont profonds (moyenne 215m).
	5b		Biseau sec du Crétacé BSC	91	50 à 90	41	5,5	3,3	33	Secteur difficile : les sables Crétacé sont stériles. Les forages cherchent les zones de fracturation du socle. Taux de réussite faible.
Mio-Pliocène	6		Unités V à VII du BSC (prof. NS > 40 m) sable, sable argileux et niveaux carbonatés	200	30 à 150	48	4,3	9,3	98	
	7		Unités V à VII du BSC (prof. NS < 40 m) sable, sable argileux et niveaux carbonatés	379	20 à 650	28	9,5	11,1	96	
Eocène - Pliocène	8		Continental Terminal dans le nord du Bénin conglomérats, brèches, microconglomérats, grés, silts et argiles	8	40 à 70	12	0,2	2,8	100	Le CT est improductif, forages dans le socle sous-jacent.
Paléocène supérieur - Eocène moyen	9a		Unités III et IV du BSC argile kaolinique, marnes	145	50 à 280	22	5,3	10,4	96	Forages dans calcaires de l'Eo-Paléocène (aquifères discontinus) ou dans les sables du Crétacé.
Paléocène inférieur et moyen	9b		Unité IIb du BSC calcaire, intercalations sableuses et marneuses	67	60 à 180	22	17,4	10,8	91	
Crétacé	10		Unités I et IIa du BSC faciès variés : sable, argile, marnes, calcaire	385	35 à 165	33	16,7	9,1	94	
	11		Grès crétacé du bassin de Kandi grès grossiers, silts, argile	24	30 à 90	17	3,8	8,2	96	Les forages captent les grès du Crétacé ou les grès Cambro-Silurien (peu différenciables)
Cambro-Silurien	12a		Grès cambro-silurien du bassin de Kandi grès fin, silts, argile	66	30 à 100	14	1,3	4,8	79	
	12b		Grès cambro-silurien du bassin de Kandi (faciès Wéré) conglomérats, brèches, grès avec silts et argiles	22	30 à 90	11	1,0	4,3	73	
Cambrien - Protéro-zoique supérieur	13a		Série de la Podiega siltites et schistes argileux, jaspes rouges	0	-	-	-	-	-	
Paléozoique	13b		Série de la Mékrou argile, silts, intercalations de grès	0	-	-	-	-	-	
	14		Série du Voltaïen grès, quartzites, grès cimentés	0	-	-	-	-	-	
Cambrien - Protérozoique supérieur	15		Série de la Pendjari, série de la Podiega argilites, silts, grès fins	284	20 à 90	9	0,7	5,0	72	
	16		Série de la Podiega grès, quartzites, schistes	248	30 à 90	8	0,4	3,3	73	
	17		Quartzites de l'Atacora quartzites, schistes quartzeux	88	40 à 90	12	0,3	3,4	63	
Protérozoique supérieur	18		Groupe de Kanson schistes séricito-quartzeux, quartzites	51	35 à 100	8	0,3	3,6	86	
	19		Série de Kandé-Boukoumbé : schistes schistes, grès, conglomérats	27	30 à 75	8	0,6	3,8	70	
	20		Groupes de Tagayéyé et de Kouandé quartzites, schistes séricito-quartzeux	91	25 à 80	8	0,5	3,0	62	
Dahoméyen et protérozoïque indifférencié	21		Gneiss de la Mékrou et de Djougou gneiss à biotite, gneiss à muscovite, amphibolite schisteuse	484	25 à 90	8	0,4	2,7	69	
	22		Amphibolites et gneiss de Founogo amphibolites, gneiss, micaschistes, généralement mylonitisés	27	30 à 120	10	0,3	2,6	70	
	23		Granulites de Pototouma-Kompa granulites basiques, dolérite en filons	5	30 à 90	8	0,5	2,9	100	
	24		Granulites de Dérouvarou granulites basiques et intermédiaires, paragneiss	11	50	10	0,2	1,6	36	
	25		Complexe métamorphique gabbroique métadiabases et métagabbros, charnockites, marbre	3	-	-	-	-	-	
	26		Complexe éruptif alcalin de la Pako granite	0	-	-	-	-	-	
	27		Complexe éruptif alcalin de la Pako laves, et tufs brèches volcaniques	0	-	-	-	-	-	
	28		Complexe volcano-sédimentaire de la Pako. Roches volcaniques de composition basaltique à andésitique, brèches volcaniques	0	-	-	-	-	-	
	29		Gneiss de Lama-Kara, de Tchamba et de Binah. Orthogneiss à muscovite, gneiss à biotite, gneiss fin, amphibolites schisteuses	126	30 à 90	5	0,4	2,9	52	
	30		Gneiss de Kabré gneiss plagioclasique à amphibole, amphibolites	36	30 à 70	5	0,1	1,9	61	
	31		Migmatites de la zone axiale (Kandi) migmatites, gneiss à biotite, granite et granodiorite	352	20 à 90	9	0,4	2,9	62	
	32		Gneiss de la zone axiale (Kandi) gneiss oeillé granitique, amphibolites	9	40 à 65	10	0,5	2,7	78	
	33		Complexe de l'Alibori gneiss à biotite, amphibolites, mylonitisés	15	30 à 75	8	0,8	4,5	93	
	34		Schistes de l'Alibori granulites rétromorphosées en faciès schistes verts	1	-	-	-	-	-	
	35		Gneiss de Sansoro gneiss à muscovite, amphibolites	20	45 à 90	8	0,1	1,3	40	
	36		Mylonite de la faille de Kandi ultramylonites	17	30 à 60	10	2,2	4,2	59	
	37		Faciès de la Wé-wé migmatites granitoïdes	54	30 à 80	8	0,4	3,5	76	
	38		Gneiss de Pira gneiss à biotite, quartzites	332	25 à 80	12	0,7	4,0	60	
	39		Granite de Waro-Maro granite, syénite	8	40 à 60	6	0,6	2,8	100	
	40		Granite du Couffo granite à biotite, charnockites	19	30 à 70	10	0,2	4,1	42	
	41		Sillon gneissique de l'Ouémé gneiss à biotite, diorite, granite-gneiss	190	20 à 90	8	0,3	3,3	55	
	42		Migmatites granitiques de Nikki-Pérérè gneiss, pyroxénite, syénite, granite	381	20 à 120	9	0,5	3,3	60	
	43		Gneiss migmatitiques du Dahoméyen gneiss à biotite, intercalations granitiques et amphibolitiques	622	25 à 135	10	0,5	3,5	62	
	44		Migmatites indifférenciées du Dahoméyen gneiss alcalins, filons de pegmatites	46	40 à 80	13	0,2	3,3	43	
	45a		Volcano-sédimentaire du Daho-Mahou dépôt terrigènes : conglomérats, grès et siltites, à débris du socle et volcani	11	40 à 65	8	0,3	4,4	64	
	45b		Basaltes du Daho-Mahou basalte, brèche basaltique, diabases	0	-	-	-	-	-	
Intrusions tardives	46		Granite intrusif (1ère à 3ème phase) granite porphyrique, granodiorite	143	30 à 90	7	0,4	2,9	57	

Figure 38: Legend of the Hydrogeological map of Benin (Lucien et al. 2012) - lithology

A.2 Lithology of the drillings near the reference piezometers

Upper depth	Lower depth	Description
0	6.4	Red laterite
6.4	30.7	Red to yellow silt + kaolin + gravel
30.7	38.9	Coarse sand
38.9	42.9	Sand + kaolin
42.9	85.33	Fine sand
85.33	87.49	Green clay

Table 8: CEG SAKETE, piezometer n°1 (950m away from the reference piezometer)

Upper depth	Lower depth	Lithology	Description
0	5	Medium sand	Clayey-lateritic sand
5	12	Sandstone	Sandstone and clayey lateritic concretion
12	23	Clay	White, plastic, ochre yellow beige plastic clay
14	19		Beige Clay
19	23		Beige Clay
23	78	Clay sand	Coarse yellow clayey sand, fine yellow sand
26	36		Rough sand (dewatered)
36	39		Coarse sand
39	48		Medium to coarse sand
48	65		Medium clayey Sand
65	76		Fine white sand
76	78		Clayey sand
78	82	Medium sand	Fine yellow clayey sand
82	88	Medium sand	Silty medium white sand + grey clay index
88	90.7	Clay	Sandy grey clay + aquifer cave

Table 9: CEG SAKETE, piezometer n°2 (1540m away from the measurements)

Upper depth	Lower depth	Lithology	Description
0	6	Clay	Red clay
6	17	Sandy Clay	Slightly sandy red clay
17	19	Gravel	Coarse sand and small gravel
19	43	Clay	Red Clay, coarse sand and small white quartzous gravel
43	49	Fine sand	Coarse sand with fine sand + clay
49	55	Clay	Whitish clay and very fine pinkish sand
55	62	Clay	Beige clay and very fine yellowish sand

Table 10: EPP BAODJO, piezometer n°3 (reference piezometer)

Upper depth	Lower depth	Lithology	Description
0	13	Clay sand	Red clayey sand
13	18	Clay	Purple clay
18	22	Sandy Clay	Purple sandy clay
22	24	Medium sand	Medium purple sand
24	26	Clay sand	Medium clayey sand
26	30	Clay	White clay
30	34	Clay sand	White clayey sand
34	37	Clay	White clay
37	40	Clay Sand	Purple clayey sand
40	48	Clay	Purple clay
48	55	Clay	White clay
55	62	Medium sand	Medium sand
62	70.2	Clay	Purple clay

Table 11: EPP BAODJO, piezometer n°4 (600m away from the measurements)

Upper depth	Lower depth	Lithology	Description
0	18	Gravelly laterite	Laterite
18	39	Clay	Yellow beige clay
39	42	Clay	Sandy clay
42	47	Clay	Yellow beige clay
47	48	Fine sand	Fine sand
48	50	Clay	Yellowish beige clay
50	55	Clay	Grey clay

Table 12: ISSALE-IBERE, piezometer n°5 (reference piezometer)

Upper depth	Lower depth	Lithology	Description
0	10	Armoured Laterite	Red laterite
10	17	Gravely Laterite	Reddish sandy laterite
17	27	Clay	Lateritic sandy ochre clay
27	32	Medium sand	
32	33	Coarse sand	Clay
33	55	Sandy clay	
55	73	Medium sand	Whitish medium to coarse sand

Table 13: MAIRIE, piezometer n°6 (reference piezometer)

Upper depth	Lower depth	Description
0	6	Terre de barre
6	34	Sandy clay
34	55	Clayey sand

Table 14: MAIRIE, piezometer n°7 (230m away from the measurements)

Upper depth	Lower depth	Lithology	Description
0	7	Sandy clay	Red brown sandy clay
7	24	Sandy clay	Brown sandy clay
24	30	Medium sand	Beige sand
30	33	Medium sand	Beige sand
33	35	Medium sand	Coarse sand with clay layers
35	37	Medium sand	Purplish sand
37	41	Sandy clay	Grey clay
41	44	Medium sand	Beige sand with clay layers
44	46.5	Medium sand	Yellowish brown sand
46.5	48	Clay	Compact grey purplish clay

Table 15: MAIRIE, piezometer n°8 (1040m away from the measurements)

Upper depth	Lower depth	Lithology
0	12	Armoured laterite
12	26	Clay
26	30	Clayey sand
30	48	Medium sand
48	61	Clay

Table 16: TAKON, piezometer n°9 (reference piezometer)

Upper depth	Lower depth	Lithology	Description
0	19	Clayey sand	Red clayey sand
19	25	Sandy Clay	Purple sandy Clay
25	37	Medium sand	Medium purple sand
37	43	Medium sand	Medium to coarse grey sand
43	46	Clayey sand	White clayey sand
46	48	Clay	White clay
48	50	Clayey sand	White clayey sand
50	58	Medium sand	Medium grey sand
58	60	Sandstone	Sandstone

Table 17: TAKON, piezometer n°10 (660m away from the measurements)

Upper depth	Lower depth	Lithology
0	6	Sandstone
6	24	Clay
24	30	Medium sand
30	42	Clay
42	61	Fine sand

Table 18: TAKON, piezometer n°11 (1340m away from the measurements)

Upper depth	Lower depth	Lithology	Description
0	1	Soil	Topsoil
1	6	Gravely laterite	Laterite
6	24.7	Sandy clay	Sandy Clay
24.7	30.4	clay	Coloured clay
30.4	37.6	Clay	Sandy clay
37.6	50.6	Medium sand	Coarse sand
50.6	55	Clay	Grey clay

Table 19: MALAHOUI, piezometer n°12 (reference piezometer)

A.3 Conduct of the water sampling campaign

A.3.1 Issale-Ibere

- Static water level: 25.93 m, the 16-03-22, 7:25
- Total depth of the borehole: 37 m
- Depth of the pump: 35 m

For this site, the borehole was emptying too fast, so it was emptied 3 times before doing the sampling. The conductivity was still measured to verify the validity of the sampling.

- 1^{st} measure: 0.108 mS/cm, 8h05
- After the 1^{st} emptying of the well: 0.105 mS/cm, 10:10
- After the 2^{nd} emptying of the well: 0.98 mS/cm, 10:34
- After the 3^{rd} emptying of the well: 0.92 mS/cm, 10:49

A.3.2 Takon

- Static water level: 35.97 m, the 16-03-22, 15:15
- Total depth of the borehole: 61.6 m
- Depth of the pump: 55 m
- Estimated flow rate: 0.976 L/s

Time	Conductivity [mS/cm]	Temperature [°C]
15:45	0.212	30.1
15:47	0.152	28.95
15:49	0.155	29
15:51	0.153	29
15:53	0.144	29
15:55	0.135	29.1
16:00	0.127	29
16:05	0.126	29
16:10	0.12	29
16:15	0.118	29.1
16:20	0.112	29.1
16:25	0.122	29.4
16:30	0.108	29
16:35	0.105	29
16:40	0.105	29
16:45	0.105	29

A.3.3 CEG Sakete

- Static water level: 28.27 m, the 16-03-22, 17:18
- Total depth of the borehole: 68 m
- Depth of the pump: 35 m
- Estimated flow rate: 1.039 L/s

Time	Conductivity [mS/cm]	Temperature [°C]
17:48	0.054	29.8
17:50	0.051	28.8
17:52	0.05	28.8
17:54	0.05	28.8
17:56	0.05	28.8
17:58	0.05	28.8
18:00	0.053	28.8
18:05	0.056	28.8
18:10	0.055	28.8
18:15	0.055	28.7
18:20	0.055	28.7

A.3.4 EPP Baodjo

- Static water level: 39.25 m, the 17-03-22, 8:30

- Total depth of the borehole: 78.29 m
- Depth of the pump: 50 m
- Estimated flow rate: 0.693 L/s

Time	Conductivity [mS/cm]	Temperature [°C]
09:02	0.06	29.4
09:04	0.05	27.9
09:06	0.049	27.9
09:08	0.048	28
11:11	0.049	31.9
11:13	0.049	28.1
11:15	0.048	28
11:20	0.048	27.9
11:25	0.048	27.9
11:30	0.049	28
11:35	0.048	28
11:40	0.0485	28.1
11:45	0.0485	28
11:50	0.049	28

A.3.5 Malahoui

- Static water level: 12.71 m, the 17-03-22, 14:14
- Total depth of the borehole: 39.8 m
- Depth of the pump: 20 m
- Estimated flow rate: 1.039 L/s

Time	Conductivity [mS/cm]	Temperature [°C]
14:31	0.043	31.4
14:33	0.043	29.2
14:35	0.046	29.1
14:37	0.047	29.1
14:39	0.047	29.1
14:41	0.047	29.1
14:46	0.047	29.1
14:51	0.047	29.2
14:56	0.047	29.2
15:01	0.047	29.1
15:06	0.048	29.1

A.3.6 Mairie

- Static water level: 26.09 m, the 17-03-22, 16:07
- Total depth of the borehole: 112.13 m
- Depth of the pump: 35 m
- Estimated flow rate: 0.887 L/s

Time	Conductivity [mS/cm]	Temperature [°C]
16:26	0.121	33.1
16:28	0.284	29.6
16:30	0.253	29.5
16:32	0.208	29.6
16:34	0.101	29.6
16:36	0.098	29.6
16:38	0.098	29.5
16:40	0.098	29.5
16:45	0.098	29.5
16:50	0.097	29.5
16:55	0.097	29.5
17:00	0.097	29.5

A.3.7 Hétin-Sota

The borehole for this site was artesian, so there was no need to wait for a stabilization of the parameters.
However, the electric conductivity and temperature were still measured : 0.968 mS/cm and 50.3 °C (the 29-03-22, 17:37).

A.4 Results of the analysis of the water samples

ID	Name	Conductivity (μS/cm, 25°C)	Temperature (°C)	pH	Total hardness	TAC	Ca^{2+}
		μS/cm	°C		°f	°f	mg/L
1	CEG SAKETE	52.6	14.6	5.00	1.2	0.6	3.83
2	ISSALE IBERE	93.1	14.7	5.72	3.3	2.3	11.03
3	EPP BADUDJO	48.9	15.0	5.08	0.9	0.7	1.57
4	TAKON	85.8	15.5	5.69	2.5	2.0	7.95
5	AKPRO MISSERETE	94.1	15.8	4.78	1.7	0.3	4.24
6	MALAHOUI	44.8	16.2	4.71	1.0	0.1	2.27
7	HETTIN SOTA	953.1	17.3	7.93	4.0	33.1	11.53

ID	OH^-	CO_3^{2-}	HCO_3^-	Free CO_2	Fe	Fe (pH < 2)	Mn	Mn (pH < 2)	SiO_2	K^+	Li^+	Mg^{2+}
	mg/L	mg/L	mg/L	mg/L	mg/L	mg/L	mg/L	mg/L	mg/L	mg/L	mg/L	mg/L
1	0.00	0.00	7.93	55.48	n.d.	0.55	0.02	0.02	26.80	0.20	n.d.	0.67
2	0.00	0.00	28.17	37.56	0.09	0.25	0.01	0.01	40.72	1.08	0.02	1.35
3	0.00	0.00	9.05	52.65	0.02	0.04	0.02	0.02	25.59	0.37	n.d.	1.15
4	0.00	0.00	24.52	35.03	0.05	4.82	0.09	0.09	33.23	0.90	0.03	1.35
5	0.00	0.00	4.67	54.25	n.d.	0.07	0.02	0.02	27.41	0.23	n.d.	1.48
6	0.00	0.00	2.41	32.87	0.04	0.05	0.02	0.02	26.14	0.22	n.d.	0.97
7	0.01	1.88	399.95	3.29	0.06	0.06	n.d.	0.01	37.81	13.83	0.06	2.72

ID	Na^+	NH_4^+	Sr_2^+	Br^-	Cl^-	F^-	NO_2^-	NO_3^-	PO_4^{3-}	SO_4^{2-}	$\delta^{18}O$	δ^2H
	mg/L	mg/L	mg/L	mg/L	mg/L	mg/L	mg/L	mg/L	mg/L	mg/L	‰	‰
1	5.04	n.d.	n.d.	n.d.	10.03	n.d.	n.d.	n.d.	n.d.	4.50	-3.22	-13.8
2	9.16	n.d.	n.d.	n.d.	9.74	0.06	n.d.	3.80	12.10	3.44	-3.28	-14.4
3	5.63	n.d.	n.d.	0.06	10.48	n.d.	n.d.	0.85	n.d.	0.54	-3.07	-13.4
4	5.69	n.d.	0.28	n.d.	12.12	0.22	n.d.	0.71	n.d.	3.58	-3.1	-14
5	9.23	n.d.	n.d.	0.05	10.06	0.01	n.d.	27.45	n.d.	0.48	-2.95	-13.2
6	3.55	n.d.	n.d.	n.d.	7.75	0.02	n.d.	7.48	n.d.	0.23	-3.17	-14.2
7	191.42	0.82	0.42	1.10	108.63	3.39	n.d.	n.d.	n.d.	0.10	-4.62	-23.5

Table 20: Results of the analysis of the water samples

A.5 Hydrochemical diagrams

A.5.1 Diagrams of the water samples collected during the internship

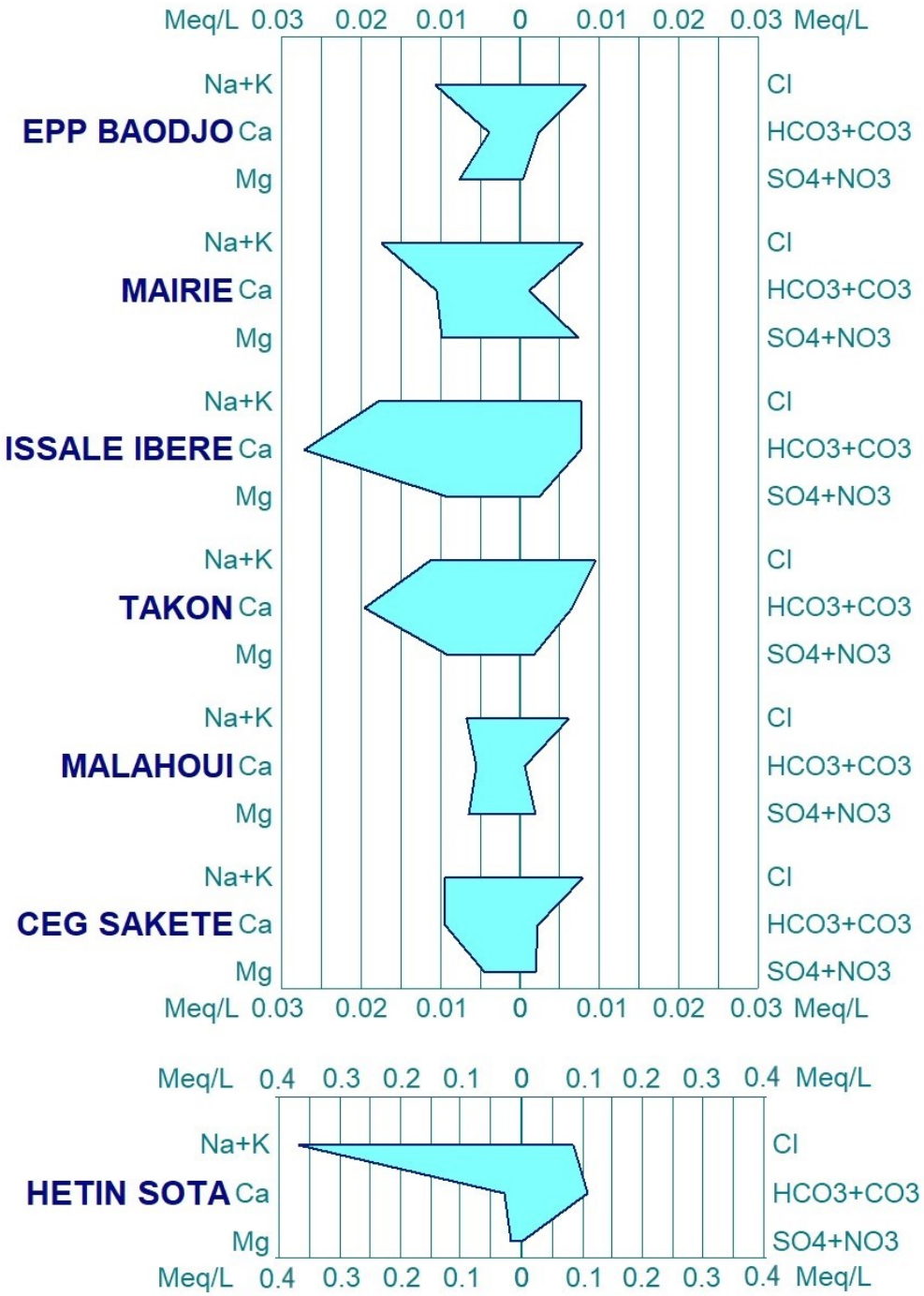

Figure 39: Stiff diagram of the water samples collected during the internship, separated into water from the Mio-pliocene aquifer (up) and the water from Hettin-Sota (down)

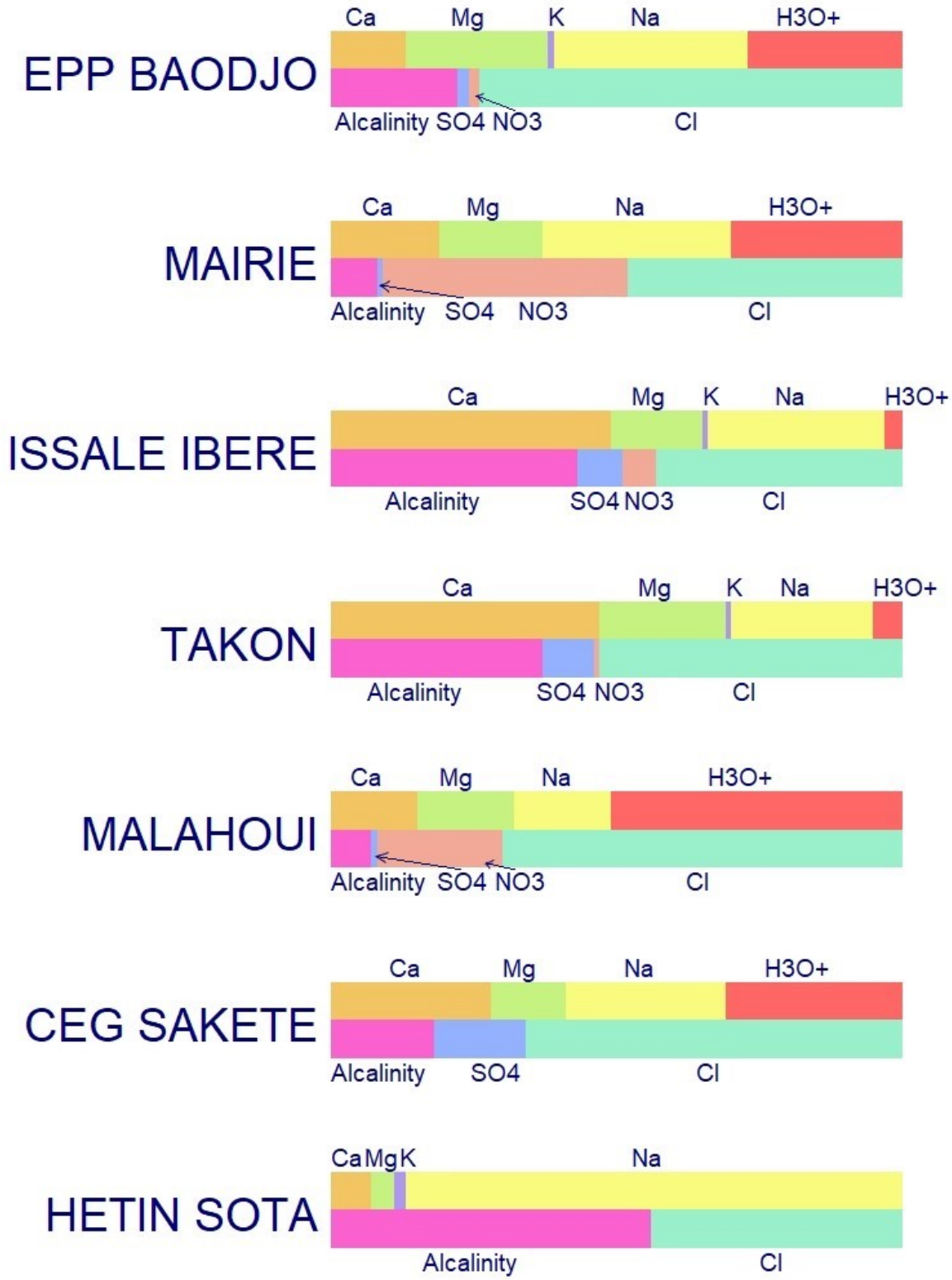

Figure 40: Stabler diagram of the water samples collected during the internship

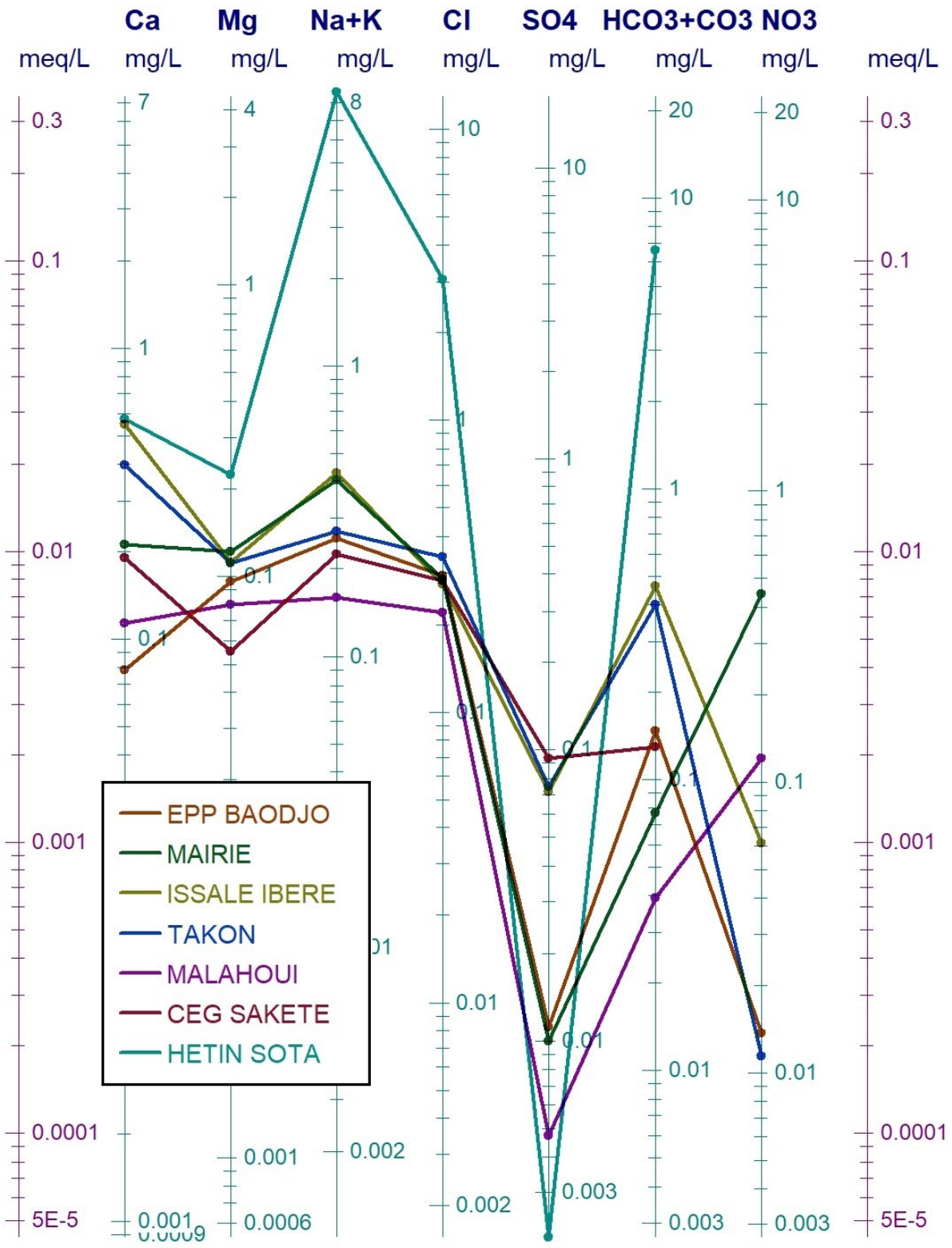

Figure 41: Schöller-Berkaloff diagram of the water samples collected during the internship

A.5.2 Diagrams of the water samples from Abdoukarim Alassane et al. 2015

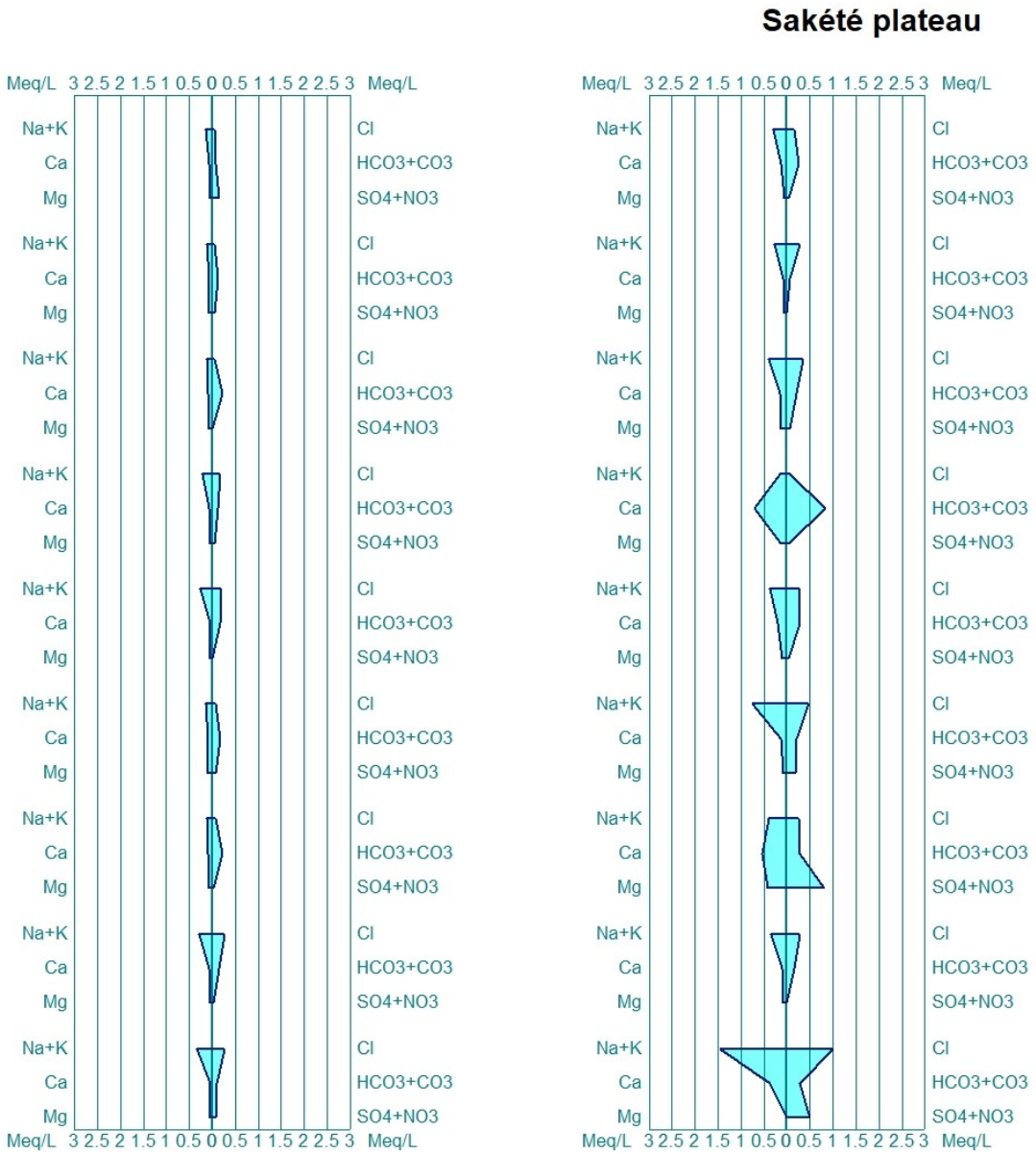

Figure 42: Stiff diagram of the water samples from Abdoukarim Alassane et al. 2015, samples from the Sakété plateau, sorted by growing electrical conductivity

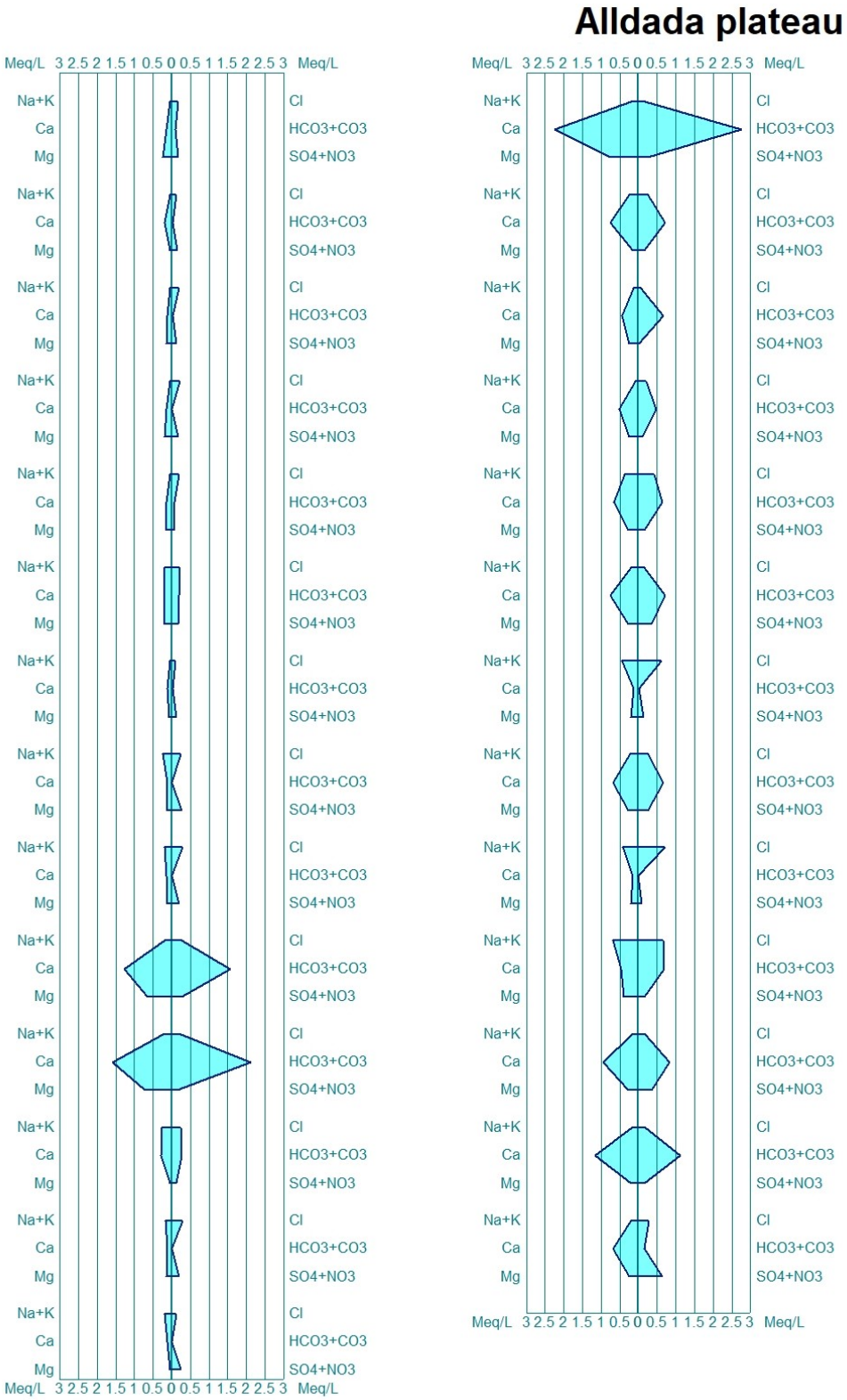

Figure 43: Stiff diagram of the water samples from Abdoukarim Alassane et al. 2015, samples from the Allada plateau, sorted by growing electrical conductivity